2009

# Tungsten trioxide and titanium dioxide photocatalytic degradations of quinoline

Laine Stewart
*Iowa State University*

**Tungsten trioxide and titanium dioxide photocatalytic degradations of quinoline**

by

**Laine Kincaid Stewart**

A thesis submitted to the graduate faculty

in partial fulfillment of the requirements for the degree of

MASTER OF SCIENCE

Major: Organic Chemistry

Program of Study Committee:
William Jenks, Major Professor
Nicola Pohl
Theresa Windus

Iowa State University

Ames, Iowa

2009

# TABLE OF CONTENTS

# Chapter 1
# General Introduction

## 1.1 Introduction

The rapidly increasing world population has placed a huge demand on our planet, both in terms of exploitation of natural resources and in addition of toxic chemicals to our environment. Groundwater contamination is one of the primary modes through which humans are exposed to toxic chemicals, so the elimination of hazardous chemicals in our water supply is extremely important to the survival and prosperity of the human race[1,2]. The greatest contributors to the pollution problem are industrial/military installations and agricultural pollutants. Some of the general classes of compounds of concern include solvents, chlorinated volatile organic compounds, pesticides, polychlorinated biphenyls, chlorinated phenols, dioxins, dibenzofurans, petroleum byproducts, asbestos, arsenic compounds, radionuclides, salts, and heavy metals. Specific compounds of concern include, but are not limited to: chlorinated aromatics (4-chlorophenol, pentachlorophenol, p-chlorobenzene), chlorinated aliphatic hydrocarbons (carbon tetrachloride, dichloromethane, chloroform, methyl chloroform, trichloroethylene, perchloroethylene, ethylene dichloride, vinyl chloride, and hexachlorocyclopentadiene) and pesticides like DDT, lindane, and kepone. Heavy metals, nitrates, and organometallic compounds (particularly tin compounds) are the most common inorganic sources of pollution, both from industrial and agricultural sources.[1]

Hazardous waste at military facilities is one of the greatest concerns related to waste remediation. In the past, toxic chemicals have been disposed of in lagoons, dump sites, and underground storage tanks. As a result of these behaviors, neighboring water supplies have become contaminated with heavy metals, byproducts of weapons manufacture, military vehicle and aviation fuel, degreasers, and solvents. Hazardous waste at military facilities delays the conversion of military installations into civilian facilities, and will take decades and tens of millions of dollars to accomplish[1].

Fertilizer run-off from large farms cause overgrowth of natural flora in water supplies, which can not be removed by natural processes[2]. Algal blooms and other overgrowths rob water supplies of oxygen and cause the death of fish and other animals that rely on that body of water for survival. Although prevention of introduction of these chemicals into water supplies is critical to any clean-up efforts, remediation of the current damage is essential to the recovery of natural ecosystems.

In order to help restore natural ecosystems and remediate the damage done to the environments, methods must be developed to safely remove these chemicals from the environment. No one method is suitable for the removal of the multitude of different types of compounds currently polluting our water supplies. Current physical methods for the removal of waste including ion exchange, distillation, filtration, and reverse osmosis, although these methods are only effective on water-insoluble or inorganic compounds, which is only a small portion of the molecules of concern[1]. Current chemical methods for removal of organic pollutants include anaerobic digestion, high temperature chemical incineration, and physicochemical methods. Chemical oxidation is a promising physicochemical method that uses highly oxidizing reagents to convert toxic organic molecules into carbon dioxide, water, and fully oxidized inorganic ions such as sulfates and nitrates. Chemical oxidation allows noxious organic compounds to be converted into species that can easily be removed by physical methods such as filtration and distillation.

Chemical oxidation processes can be divided into two main classes: conventional and advanced. Conventional oxidation processes utilize wet chemical oxidizing agents such as ozone, Fenton chemistry ($Fe^{3+}/H_2O_2$), persulfate, and permanganate. These methods are effective for the oxidative degradation of organic compounds, although their toxicity and safety hazards limit their usefulness. In some cases, the intermediates produced by these processes are more toxic than the original compounds[3].

A more viable and extensively studied alternative to conventional oxidation pathways are advanced oxidation processes, including radiolysis, sonolysis, and photolysis. Advanced

oxidation processes (AOPs) create oxidants *in situ* with high oxidation power[4]. The most promising of these methods is the use of photolytic processes for degradation of organic pollutants. The most common methods for photolytic degradation of organic compounds are direct photolysis, photolysis with ozone, photodegradation with UV/$H_2O_2$, and photocatalysis (including semiconductor photocatalysis)[5].

## 1.2 Thesis Organization

This thesis is divided into four chapters. Chapter one in a general introduction to advanced oxidation processes for the degradation of organic molecules, primarily the use of semiconductor photocatalysis for the degradation of organic pollutants, though a brief background of other processes is presented. Chapter two concerns the use of $S_8$-$TiO_2$ for the photocatalytic degradation of quinoline, a representative organic molecule. Although other sulfur-doped photocatalysts have been developed, $S_8$-$TiO_2$ may prove to be a very promising photocatalyst as it shows similar degradative ability to S-$TiO_2$ prepared with thiourea, but is simpler and less expensive to prepare. Chapter three presents the degradation of quinoline with nanometer-sized $WO_3$ and a WC-$WO_3$ composite photocatalyst. Although the degradative ability of $WO_3$ was not enhanced by addition of WC, analysis of the degradative ability and product ratio provides insight into the photochemistry of $WO_3$ photocatalysts.

## 1.3 Advanced Oxidation Processes

### 1.3.1 $H_2O_2$/UV process

Hydroxyl radicals can be generated from hydrogen peroxide by photolysis with UV light (equation 1.1).

$$H_2O_2 \xrightarrow{hv} 2\,HO^{\bullet} \qquad (1.1)$$

The hydroxyl radical can further react with hydrogen peroxide to generate the hydroperoxyl radical, which can also act as an oxidizing agent (equation 1.2).

$$H_2O_2 + HO^{\bullet} \longrightarrow H_2O + HOO^{\bullet} \qquad (1.2)$$

Hydroxyl radicals can further react with organic molecules through a variety of pathways-hydrogen abstraction, electron transfer, and electrophilic addition. Hydrogen peroxide is a cheap oxidant and is completely miscible with water, but the absorption coefficient and quantum efficiency of hydroxyl radical production is low at $\lambda > 250$ nm[4].

### 1.3.2 Ozone/UV process

Ozone is strong oxidant (redox potential of 2.07 V at pH 1) and is thus useful for the degradation of some organic molecules in water[6,7]. However, as with hydrogen peroxide, UV photolysis generates hydroxyl radicals (equation 1.3)[8].

$$O_3 \xrightarrow{h\nu < 310\ nm} O_2 + O(^1D)$$
$$O(^1D) + H_2O \longrightarrow 2\ HO^{\bullet} \qquad (1.3)$$

Hydroxyl radical may also be formed through the following pathway (equation 1.4).

$$O_3 + H_2O \xrightarrow{h\nu} H_2O_2 + O_2 \qquad (1.4)$$

Hydroxyl radicals will then be formed from the hemolytic photolysis, as in equation 1.1.

### 1.3.3 Photo-Fenton Reaction

The Fenton reaction is an efficient method of generating hydroxyl radicals via reaction of hydrogen peroxide with $Fe^{2+}$ (equation 1.5)[9].

$$Fe^{2+} + H_2O_2 \longrightarrow Fe^{3+} + HO^- + HO^{\bullet} \qquad (1.5)$$

The Fenton reagent has been used for efficient degradation of pollutants in both soil and water. An even more effective system for the oxidative degradation was developed by the application of UV/Vis irradiation to the traditional Fenton reaction (equation 1.6)[10,11,12]. Either method of Fenton degradation is usually quite effective in the degradation of organic molecules. However, iron salts are pollutants themselves and thus must be removed from the reaction mixture by precipitation as $Fe(OH)_3$.

$$Fe^{2+} + H_2O \longrightarrow Fe^{3+} + H^+ + HO^{\bullet} \qquad (1.6)$$

### 1.3.4 Sonolysis

Upon irradiation with high intensity sound or ultrasound irradiation, a process called acoustic cavitation occurs[13]. Gas bubbles are formed in solution, which rapidly implode creating small, localized intense conditions in otherwise cold solutions with temperatures of nearly 5000K and pressures of 1000 atm. These extreme conditions lead to the dissociation of $H_2O_2$ or $H_2O$ to reactive species such as hydroxyl radicals, etc. Sonolysis has been used for the degradation of toxic organophosphorus compounds to $CO_2$, $H_2O$, and $H_3PO_4$[14,15].

### 1.3.5 Radiolysis

Radiolysis is a general class of reaction that uses high-energy radiation for chemical reactions or bond cleavage[16]. Short-wavelength radiation, a beam of accelerated charged particles (electrons, protons, etc.), or the radiation produced from the decay of radioactive nuclei (alpha, beta, or gamma radiation) are commonly used for radiolysis. Organic molecules can either be degraded through direct or indirect irradiation in radiolysis. Generally, degradation takes place by indirect interaction with irradiation because of the low concentration of molecules in solution (i.e. interaction with hydroxyl radicals and other reactive species by irradiation).

### 1.3.6 Semiconductor Photocatalysis

The use of semiconductors as photocatalysts for the mineralization of organic molecules to $CO_2$, $H_2O$, and inorganic ions (sulfate, nitrate, etc.) has arisen as a viable alternative to the methods described above[1,4]. One notable advantage to the use of semiconductor photocatalysts is that they are nearly always water insoluble and can be easily removed from the reaction medium once a reaction is complete or can be coated on to various substrates. Semiconductor photocatalysts are often very stable under aqueous conditions and resistant to photochemical degradation. A number of different semiconductors are available, but only a few of them are well-suited to the degradation of organic molecules and have been heavily studied, namely $TiO_2$, $WO_3$, ZnO, CdS, ZnS, and $Fe_2O_3$[17]. The degradation of organic molecules will be discussed in more detail in Chapters 2 and 3.

The oxidation potential and the band gap energy are critical to the effectiveness of a given semiconductor as a photocatalyst for the remediation of organic molecules. The electronic structure of semiconductors is characterized by a filled valence band and empty conduction band. The energy difference between the valence band and the conduction band is called the band gap energy, denoted $E_g$. When a photon with an energy greater than or equal to the band gap energy is absorbed by the semiconductor an electron, $e_{cb}^-$, is promoted from the valence band (VB) to the conduction band (CB), leaving a hole ($h_{vb}^+$) behind in the valence band[18]. The conduction band electrons and valence bond holes may recombine (eliminating the energy as heat), become trapped at meta-stable trap sites on the semiconductor surface, or with molecules adsorbed on the surface of the semiconductor.

Without the presence of suitable electron or hole scavengers, the electron and hole will recombine within a few nanoseconds. If organic molecules are adsorbed to the surface or other hole or electron scavengers are available, recombination will be at least partially prevented and subsequent redox reactions can occur. Valence bond holes are oxidants and conduction band electrons are reducing agents. In order for these species to be effective in the degradation of organic molecules, the valence band hole must be sufficiently positive to generate absorbed $HO^\bullet$ radicals, and the redox potential of the conduction band hole must be sufficiently negative to reduce adsorbed $O_2$, the most common electron sink, to superoxide. Titanium dioxide has been shown to the most active and promising semiconductor for photocatalysis[1].

## 1.4 Titanium dioxide photocatalysis

### 1.4.1 Introduction

Titanium dioxide has proven to be the most promising photocatalyst for degradation of organic pollutants for a variety of reasons. Titanium dioxide has a high oxidation potential and a band gap that allows for the absorption of the UV portion of sunlight. Unfortunately, the UV portion of terrestrial sunlight only accounts for less than 10% of the solar spectrum. However, titanium dioxide has many other advantages. $TiO_2$ is

biologically and chemically inert, photostable, inexpensive, and reusable with a high turnover rate. It is also easy to alter the particle size as well as absorption range by doping with other elements, the two key elements to the photocatalytic activity of titanium dioxide[1]. Doping of titanium dioxide to extend the band gap to longer wavelengths will be discussed in Chapter 2.

### 1.4.2 General mechanism of initial steps[1]

Typical photocatalytic degradations with titanium dioxide are performed with oxygen-saturated aqueous suspensions of $TiO_2$. When UV irradiation matches or exceeds the band gap energy of titanium dioxide, a valence band (VB) hole and conduction band (CB) electron are generated (equation 1.7), which can then go on to react with oxygen, water, and organic molecules in the solution (equations 1.8-1.15).

$$TiO_2 + h\nu \rightarrow e^-_{cb} + h^+_{vb} \quad (1.7)$$

$$H_2O_{ads} + h^+_{vb} \rightarrow HO^\bullet_{ads} + H^+ \quad (1.8)$$

$$O_2 + e^-_{cb} \rightarrow O_2^{\bullet-} \quad (1.9)$$

$$O_2^{\bullet-} + H^+ \rightarrow HO_2^\bullet \quad (1.10)$$

$$HO_2^\bullet + HO_2^\bullet \rightarrow H_2O_2 + O_2 \quad (1.11)$$

$$H_2O_2 + e^-_{cb} \rightarrow HO^\bullet + HO^- \quad (1.12)$$

$$D + h^+_{vb} \rightarrow D^{\bullet+} \quad (1.13)$$

$$A + e^-_{cb} \rightarrow A^{\bullet-} \quad (1.14)$$

$$e^-_{cb} + h^+_{vb} \rightarrow TiO_2 + \text{heat} \quad (1.15)$$

The valence band hole can go on to react with water adsorbed to the titanium dioxide surface to generate adsorbed hydroxyl radicals (equation 1.8). This is the main mechanism for formation of hydroxyl radicals, which are believed to be the main oxidizing species in many circumstances[19]. The conduction band electron reaction with molecular oxygen generates superoxide (equation 1.9), which can produce more hydroxyl radicals as downstream products via formation of hydrogen peroxide (equations 1.10-1.12), which can react with organic molecules in solution. Reductive titanium dioxide

chemistry is studied much less frequently because the reducing power of the CB electron is much less than the oxidative power of the VB hole[17].

The VB hole can also react directly with a donor organic molecule (**D**) (equation 1.13) and the CB electron can react directly with an acceptor (**A**) organic molecule (equation 1.14). The final equation in this scheme describes the recombination of the conduction band electron and valence band hole to generate heat. This reaction is the major process occuring in an excited semiconductor, accounting for over 90% of charge carriers formed and competing with all "productive" chemistry in the photocatalyst system[20]. The overall process is also represented graphically in figure 1.

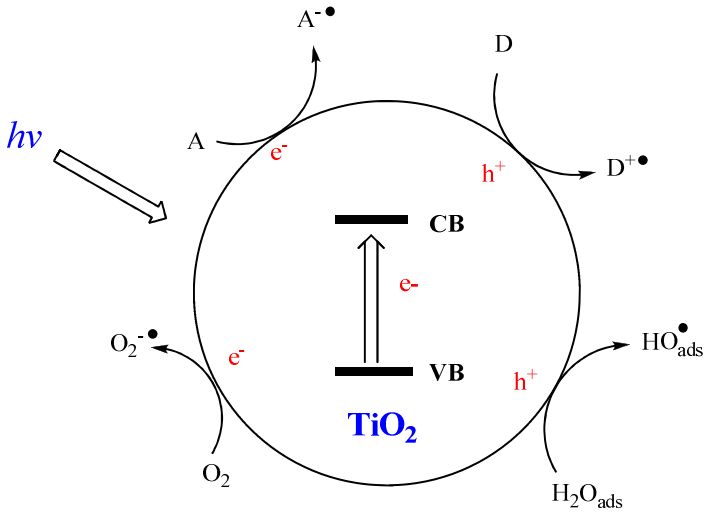


**Figure 1. Excitation of Titanium Dioxide.**

Prevention of surface recombination is one of the most important elements to enhancing photocatalytic activity, and extensive research to understand surface recombination and processes to reduce it is currently underway. To prevent recombination, an oxidizing agent (usually molecular oxygen) is added to the solution to trap the conduction band electron as superoxide. Even without the deliberate addition of molecular oxygen this process will still occur to some extent in aqueous solutions in air. Molecular oxygen is an ideal electron trap due to its high reduction potential and the fact that downstream products of the reaction of molecular oxygen and the conduction band electron include

hydroxyl radicals, which are a highly oxidizing species and is stoichiometrically required for oxidation of organic molecules. Because of this, equation 1.9 becomes very important in aqueous photocatalysis[1].

In addition to oxidative degradation by hydroxyl radicals or valence bands holes, direct single electron transfer (SET) also plays a role in the degradation of some organic molecules. Jenks et al.[21,22] has suggested that the ring-opened products of the $TiO_2$ photocatalytic degradation of 4-chlorophenol is due to direct single electron transfer, and not reaction with hydroxyl radical. In phenol and catechols (1,2-benzenediols) ring-opened products attributed to SET chemistry are often seen. Molecular oxygen attacks the adsorbed molecule to form two carboxylic acids via a dioxetane intermediate[22].

### 1.4.3 Effects on titanium dioxide photodegradations

#### 1.4.3.1 Crystal Phase

Titanium dioxide exists in three crystal phases: anatase, rutile, and brookite. Brookite is the least studied of the three, because it is the most difficult to obtain in pure form. Anatase is generally thought of as the most photocatalytically active phase, though extensive study has also been done on the rutile phase.

Rutile was the first crystal phase to be studied in detail, and much of the fundamental experimental and theoretical work on $TiO_2$ photocatalysis was using rutile titanium dioxide. Rutile, with a band gap of 3.0 eV (418 nm), would seem to be a more ideal photocatalyst than anatase (3.2 eV, 387 nm), but it has been shown to be a less active photocatalyst than anatase[23]. It is thought that rutile is a less active photocatalyst than anatase due to the tighter packing in the rutile crystal structures, which has fewer defects to trap photoexcited holes and electrons, which reduce charge carrier recombination. As a result of this, the vast majority of recent research on titanium dioxide photocatalysts has been done on the anatase phase. The higher band gap of anatase $TiO_2$ also leads to a higher oxidation potential, which can thus degrade less reactive organic molecules than rutile, but also utilizes of a smaller portion of the solar spectrum.

A mixture of anatase and rutile titanium dioxide has be shown to have greater photocatalytic activity than either phase alone. Degussa P25 is a popular commercial catalyst than contains 80% anatase and 20% rutile and is produced by high temperature sintering of $TiCl_4$ in the presence of oxygen and hydrogen[24]. The enhanced photocatalytic activity of Degussa P25 is thought to be from the ability of excited electrons generated in the anatase particles to be transferred to the rutile particles, thus minimizing charge recombination[25].

#### 1.4.3.2 Particle size effects

Titania particle size (and therefore surface area) of titanium dioxide particles has been extensively studied and shown to have a significant effect on photocatalytic activity. The surface area of the catalyst affects the number of molecules than can adsorb to the surface of the photocatalyst. Surface area also effects the rates of electron/hole recombination, as recombination is a surface process[26,27]. In general, nanometer size titanium dioxide has been shown to be the most effective (P25 has a particle size of 25-35 nm[24]), although some micrometer-sized catalysts are shown to be reasonably active. In addition to varying the size of titanium dioxide nanoparticles, different particle shapes and coatings of titanium dioxide have been utilized for photochemical degradations.

#### 1.4.3.3 Effect of pH

Particle size, surface charge, and the band edge position are also influenced by pH. The isoelectric point for titanium dioxide in water is approximately pH = 6.6[28], and thus a positive charged surface is expected at lower pH and a negatively charged surface above this pH, due to protonation or deprotonation of surface hydroxyl groups. For an n-type semiconductor such as $TiO_2$, accumulation of negative charges at the surface causes an upward band bending and thus improved transfer of photogenerated holes. In general, there was found to be less than one order of magnitude difference in the rate of degradation between pH 2 and 12[29-31], though this is highly dependent on substrate.

#### 1.4.3.4 Effect of $TiO_2$ concentration

Generally, the rate of degradation is linearly related to the amount of $TiO_2$, eventually leveling off to a steady value[32,33], although for some cases the rate can actually decrease when too much $TiO_2$ is present[34,35]. This behavior is expected with complete light absorption at the semiconductor surface. Rates increase with the amount of $TiO_2$ because more active sites are available for reaction, although when too much $TiO_2$ is present aggregation of particles can occur, which reduces the availability of reaction sites. Rates may also decrease because of increased solution opacity and light scattering.

#### 1.4.3.5 Effect of substrate concentration

Most organic molecules obey the Langmuir-Hinshelwood kinetic model, although this is not always the case, particularly if the molecule in question absorbs UV light strongly. For representative molecules like 4-chlorophenol, the reaction rate increases as the initial rate increases.[22]

#### 1.4.3.6 Effect of oxygen concentration

Since oxygen serves as a trap for the photogenerated electrons, thus inhibiting the recombination of the electron/hole pair, the concentration of dissolved molecular oxygen also affects the reaction rate. The rate of degradation is proportional to the fraction of $O^2$, up to the point of saturation.[36]

#### 1.4.3.7 Effect of reaction temperature

In general, photochemical reactions are not temperature-sensitive. Photodegradation is slightly temperature sensitive because important steps in the titanium dioxide degradations including adsorption and desportion, surface migration, and rearrangements. Activation energies of photodegradations are typically in the 5-15 kJ/mol range[36].

### 1.4.4 Titanium dioxide doping

In order to extend the absorption of titanium dioxide further into the visible range, doping of titanium dioxide has become a rapidly growing research area. A wide variety of metals

and main group elements have been introduced into titanium dioxide in hopes of extending the light absorption into the visible and/or decreasing the recombination rate. One of the first and most successful additions to titanium dioxide was the deposition of noble metals (e.g. Au or Pt) onto the surface of $TiO_2$ for water splitting into hydrogen and oxygen. The addition of small platinum particles onto the titanium dioxide surface increases the production of $H_2$, because electrons move to platinum which then reduces water to $H_2$. Platinum is especially effective for increasing degradation rates for rutile titanium dioxide, but is far too expensive to use on a large scale. Transitions metal cations have been introduced into titanium dioxide (like Cr and Fe), but they acted as recombination sites, increasing the rate of recombination instead of decreasing it[23].

Titanium dioxide composites with other metal oxides (such as $WO_3$) have also been synthesized[37]. Tungstate doping has been shown to be particularly effective in shifting the band gap into the visible (2.86 eV vs. 3.2 eV for anatase) and increasing photocatalytic activity[38].

The most recent type of titania doping uses main group elements, particularly C, N, and S. Main group elements may substitute for either titanium or oxygen in the titanium dioxide lattice or may occupy interstitial sites in the lattice. It is thought that main group elements create mid-gap levels in the electronic band structure, permitting lower energy (longer wavelength) excitations, and thus extending the band gap further into the visible spectrum[20].

### 1.4.5 Application of $TiO_2$ photocatalysis

Photocatalytic degradation of organic pollutants using titanium dioxide can be summarized by the following reaction (equation 1.16):

$$\text{Organic molecule} + O_2 \xrightarrow[h\nu \geq E_{bg}]{TiO_2} CO_2 + H_2O + \text{inorganic ions} \qquad (1.16)$$

The degradations of a huge variety of compounds have been extensively investigated. For an extensive review see Hoffmann's publication.[1] The use of titanium dioxide and other

photocatalysts to degrade organic molecules is a rapidly growing field and new discoveries and mechanistic insights are being made every day.

## 1.5 References

(1) Hoffmann, M.R.; Martin, S.T.; Choi, W.; Bahnemann, D.W. *Chem. Rev.* **1995**, *95*, 69-96.

(2) Lorch, W. *Handbook of Water Purification;* Second ed.; Ellis Horword: Chichester, 1987.

(3) Huling, S.G.; Pivetz, B.E.; United States Environmental Protection Agency: 2006.

(4) Legrini, O.; Oliveros, E.; Braun, A.M.; *Chem. Rev.* **1993**, *93*, 671-698.

(5) Halmann, M.M. *Photodegradation of Water Pollutants*; CRC Press: New York, 1996.

(6) Lelacheur, R.M.; Glaze, W.H. *Environ. Sci Technol.* **1996,** *30*, 1072-1080.

(7) Hausler, R.; Briere, F.G.; Beron, P. *Ozone Sci. Eng.* **1993**, 15.

(8) Peyton, G.R.; Glaze, W.H. *Environ. Sci. Technol.* **1988,** *22*, 761-767.

(9) Walling, C. *Acc. Chem. Res.* **1975,** *8*, 125-131.

(10) Bauer, R.; Fallmann, H. *Res. Chem. Intermed.* **1997,** *23*, 341-354.

(11) Zepp, R.G.; Faust, B.C.; Hoigne, J. *Environ. Sci. Technol.* **1992**, *26*, 313-319.

(12) Pignatello, J.J.; Sun, Y. *Water Res.* **1995,** *29*, 1837-1844.

(13) Johnson, A.J.; Hocking, P. *ACS Symp. Ser.* **1993**, *518*, 106-18.

(14) O'Shea, K.E.; Aguila, A.; Vinodgopal, L.K.; Kamat, P.V. *Res. Chem. Intermed.* **1998**, *24*, 695-705.

(15) O'Shea, K.E.; Garcia, I.; Aguilar, M. *Res. Chem. Intermed.* **1997**, *23*, 325-329.

(16) Parmon, V.; Emeline, A.V.; Serpone, N. *Intern. J. Photoenergy* **2002**, *4*, 91-131.

(17) Fox, M.A. *Chem. Rev.* **1993**, *93*, 341-357.

(18) Oppenlander, T. *Photochemical Purification of Water and Air*, Wiley-VCH: London, 2003.

(19) Murakami, Y.; Kenji, E.; Nosaka, A.Y.; Nosaka, Y. *J. Phys. Chem. B.* **2006**, *108*, 8751-8755.

(20) Thompson, T.L.; Yates, J.T. *Chem. Rev.* **2006**, *106*, 4428-4453.

(21) Li, X.; Cubbage, J.W.; Tetzlaff, T.A.; Jenks, W.S. *J. Org. Chem.* **1999**, *64*, 8509-8524.

(22) Li, X.; Cubbage, J.W.; Jenks, W.S. *J. Org Chem.* **1999**, *24*, 8525-8536,

(23) Linsebigler, A.L.; Lu, G.; Yates, Jr. J.T. *Chem. Rev.* **1995**, *95*, 735-758.

(24) Tahiri, H.; Serpone, N.; Le van Mao, R. *J. Photochem. Photobiol. A.* **1996**, *93*, 199-203.

(25) Hurum, D.C.; Gray, K.A. *J. Phys. Chem. B* **2005**, *109*, 977-980.

(26) Serpone, N.; Lawless, D.; Khairutdinov, R.; Pelizzetti, E. *J. Phys. Chem.* **1995,** *99*, 26655-16661.

(27) Calza, P.; Pelizzetti, E.; Mogyorosi, K.; Kun, R. Dekany, I. *Appl. Cat. B.* **2007**, *72*, 314-321.

(28) Augustinkski, J. *Struct. Bonding* **1988**, *69*, 1.

(29) Terzian, R.; Serpone, N.; Minero, C.; Pelizzetti, E. *J. Catal.* **1991**, *128*, 352-65.

(30) Okamoto, K.; Yamamoto, Y.; Tanaka, H.; Tanaka, M.; Itaya, A. *Bull. Chem. Soc. Jpn.* **1985**, *58*, 2015-2022.

(31) Okamoto, K.; Yamamoto, Y.; Tanaka, H.; Tanaka, M.; Itaya, A. *Bull. Chem. Soc. Jpn.* **1985**, *58*, 2023-2028.

(32) Serpone, N.; Salinaro, A. *Pure Appl. Chem.* **1999**, *71*, 303-320.

(33) Salinaro, A.; Emeline, A.V.; Zhao, J.; Hidaka, H.; Ryabchuk, V.K.; Serpone, N. *Pure Appl. Chem.* **1999**, *71*, 321-335.

(34) Aguilar, A.; O'Shea, K.E.; Tobien, T.; Asmus, K.-D. *J. Phys. Chem. A* **2001,** *105*, 7834-7839.

(35) San, N.; Hatipoglu, A.; Kocturk, G.; Cinar, Z. *J. Photochem. Photobiol. A* **2002**, *146*, 189-197.

(36) Mills, A.; Davies, R. H.; Worsley, D. *Chem. Soc. Rev.* **1993**, *22*, 417-425.

(37) Wu, Q.; Li, D.; Chen, Z.; Fu, X. *Photochem. Photobiol. A***2006**, *181*, 421-428.

(38) Song, H.; Jiang, H.; Liu, X.; Meng, G. *J. Photochem. Photobiol. A* **2006**, *181*, 421-428.

# Chapter 2

# S-$TiO_2$ Photocatalysts for the Degradation of Organic Compounds

The following chapter is modified from a paper submitted to Applied Catalysis B: Environmental and is a collaborative work with Erin Rockafellow. The research concerning $S_8$-$TiO_2$ and the initial rate comparison of $S_8$-$TiO_2$ and S-$TiO_2$ quinoline degradations with 350 nm irradiation was performed by Laine Stewart and the S-$TiO_2$ research was performed by Erin Rockafellow. The significance of the work concerning $S_8$-$TiO_2$ is much more obvious when presented in context with the research on S-$TiO_2$.

## 2.1 Introduction

The use of titanium dioxide as a photocatalyst for the degradation of organic compounds in water has received a great deal of attention.[1-6] Titanium dioxide is of particular interest because it is robust, thermally stable, non-toxic, and cheap. Upon absorption of light with sufficient energy for band gap excitation, charge separation occurs, promoting an electron ($e^-$) to the conduction band leaving a void, or hole ($h^+$), in the valence band. These photogenerated charges can migrate to the surface of the photocatalyst where charge transfer with surface-bound adsorbates and nearby molecules can occur in competition with recombination of the electron/hole pair. Nearby organic molecules can then undergo oxidative reactions by either indirect, hydroxyl-like pathways (hereafter referred to as $HO\bullet_{ads}$ to distinguish this chemistry from that of true bulk-solvated hydroxyl radicals, HO•) or single electron transfer (SET), which involves direct electron transfer from the organic molecule to the photogenerated hole ("hole attack") or potentially to another photogenerated reactive species, like HO•.[4,7-13]

Unfortunately, anatase, the most reactive phase of $TiO_2$, has a low quantum yield for oxidation steps (≤ 5%) as a result of rapid recombination of photogenerated charges. In addition, pure anatase is only able to use < 10% of the terrestrial solar spectrum because

of its wide band gap (3.2 eV), with rutile having a slightly smaller band gap (3.0 eV), but generally lower activity.

Doping $TiO_2$ with metal cations or main group elements has been shown to induce extensions of the absorption spectrum into the visible.[4,14-16] Although transition metals give the desired red shift, many of them can act as recombination centers. This reduces the semiconductor's photochemical efficiency and therefore utility as a photocatalyst.[4,9] Recent research has focused greatly on doping $TiO_2$ with nonmetal main group elements to create materials we designate as N-$TiO_2$, C-$TiO_2$, etc., with S-$TiO_2$ being the focus of this paper.[14,17-53]

The origin of the shifted absorption and its relationship to the photocatalytic chemistry is essential. Asahi originally proposed that nitrogen doping creates a delocalized mixing between the O 2p and N 2p orbitals causing a rise in the valence band.[14] Most current research supports an alternative proposal in which the dopant atom orbitals generate an isolated mid-gap level above the valence band.[13,27,33,53-56] Intuitively, this point is a key one for understanding the chemistry that these catalysts will initiate, given that oxidation is the main $TiO_2$-mediated degradation pathway. Raising the bulk valence band energy level would necessarily lower the oxidizing power of the photochemically generated hole and potentially interfere with certain reactions the pristine catalyst could perform. The role of isolated mid-gap level holes is less clear, though they also should result in low energy "hole traps" that were less chemically active than the main valence band holes. Excitation in the low energy edge of the absorption would presumably mean direct formation of such trapped holes, but UV excitation could also lead to low energy trapped holes via migration to the dopant center. It is thus apparent that at the limit of high charge mobility and rapid trapping, all excitations might have a lowered oxidation power over the undoped $TiO_2$. On the other hand, if oxidation of adsorbed substrates were competitive with charge migration within the particle, a wavelength dependence on the observed chemistry might be found.

Several key studies have reported on the differences in charge carrier mobility generated by irradiation with UV light versus visible light.[13,47,55,57] Others have recently noted wavelength-dependent chemistry for N-$TiO_2$ remediation of ethylene glycol in acetonitrile,[55] as well as C-$TiO_2$-mediated degradation of molecules with different binding abilities and oxidation potentials.[13]

To probe the photocatalytic activity of doped titania, many other studies have used dyes as chemical probes, some of which are prone to both oxidative and reductive degradation pathways and are often unrepresentatively easy to oxidize or reduce, compared to more common relevant pollutants. Dyes also absorb light is the visible region, which is an undesirable trait. The use of methylene blue, perhaps the most common of these, remains controversial for these and other reasons.[46,58,59] We prefer molecules more closely related to common pollutants such as aromatic pesticides, herbicides, manufacturing byproducts, or petroleum products that also have well-defined oxidative pathways.

In this paper, we report the an investigation of S-$TiO_2$ prepared in two ways – a conventional sol-gel preparation, and a modification of existing $TiO_2$ by annealing with $S_8$ – and an evaluation of the chemical reactivity of these catalysts in the UV and visible ranges. As chemical probes, we use three aromatic molecules with considerably different adsorption modes and modes of reactivity. These compounds, 4-methoxyresorcinol (**MR**), 1-(*p*-anisyl)neopentanol (**AN**), quinoline (**Q**), have well established patterns of oxidative reactivity.[11,60-62] By examining the partial degradation mixtures at low conversion of the starting material, reaction products can be used to distinguish between hydroxyl-type and single-electron transfer (SET) interactions with the catalyst, as shown in Scheme 1.

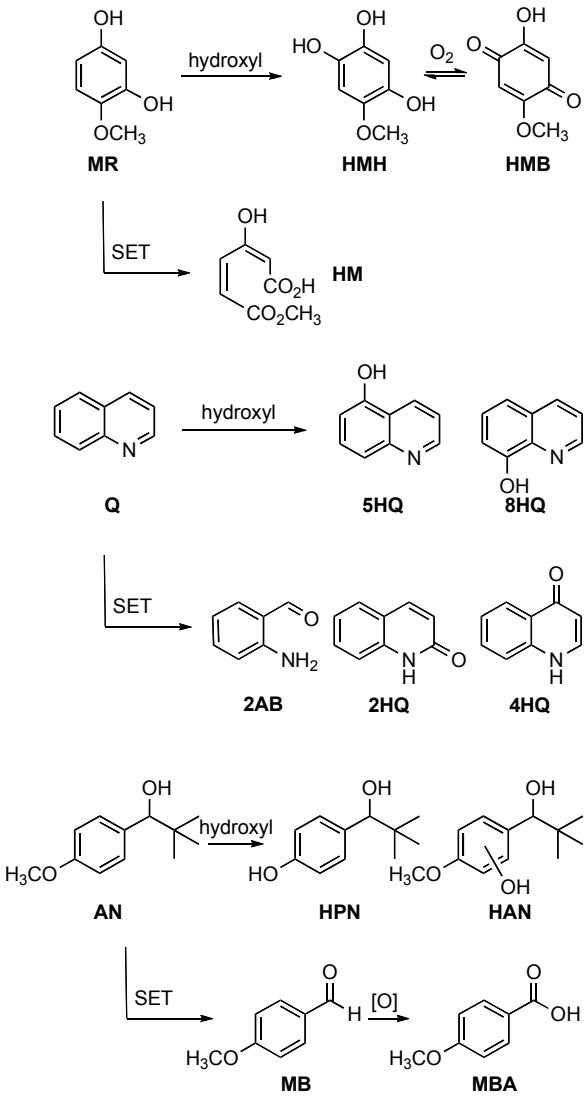


**Scheme 1.** Early photocatalytic degradation steps for **MR**, **Q**, and **AN.**

## 2.2 Experimental

### 2.2.1 Organic Materials.

Chemicals were purchased at the highest available purity and used as received, unless noted otherwise. 4-Methoxyresorcinol[63] and 1-(*p*-anisyl)neopentanol[60] were prepared by literature methods. Water was purified using a Milli-Q UV plus system with a resistivity above 18 MΩ/cm. PC500, a commercial anatase, was received from Millenium

Chemical Company, and used only for the purpose of showing the anatase pattern in the powder XRD.

**2.2.2 Photocatalyst preparation.**

Sulfur-doped titanium dioxide (S-$TiO_2$) was prepared using a lightly modified literature procedure due to Ohno.[36,44] Thiourea (53.4 g) was dissolved in 550 mL 90% ethanol followed by drop-wise addition of titanium (IV) isopropoxide (51.5 mL) and vigorous stirring to yield a white precipitate. The solution was stirred at room temperature under aerated conditions for 48 hours to allow for complete hydrolysis. Solvent was removed under reduced pressure, and the remaining white powder was annealed at 450 ˚C for 4 hours. The material was then washed thoroughly with water to remove residual surface adsorbates and any surface sulfates. S-$TiO_2$ was obtained as a vivid yellow powder. Undoped $TiO_2$ was prepared by a similar method as S-$TiO_2$ without thiourea.

A second method was also used for the synthesis of sulfur-doped titanium dioxide, designated $S_8$-$TiO_2$. Samples of undoped $TiO_2$ obtained from the previous procedure were used as the starting material. Undoped (but otherwise identically prepared) pre-annealed $TiO_2$ (5.00 g) and $S_8$ (2.00 g) were mixed and ground together thoroughly with a mortar and pestle, followed by annealing at 350 ˚C for 4 hours. (The boiling point of $S_8$ is 445 ˚C). The resulting tan powder was washed with water to remove surface adsorbates and sulfates. As a control, washing with $CS_2$ was also performed, and no color change resulted.

**2.2.3 Catalyst Characterization.**

Powder x-ray diffraction (XRD) spectra were taken with a x-ray powder diffractometer employing Cu $K_\alpha$ radiation. Surface analysis of the materials was performed by nitrogen sorption isotherms in a sorptometer. The surface areas were calculated by the Brunauer-Emmett-Teller (BET) method. X-ray photoelectron spectroscopy (XPS) was done using a multitechnique spectrometer utilizing nonmonochromatized Al K radiation with a 1 $mm^2$ sampling area. The take off angle was fixed at 45˚. Spectra were calibrated to the C1s peak at 284.7 eV. Diffuse reflectance spectra (DRS) were generated with a UV-vis

spectrometer equipped with a diffuse reflectance accessory. MgO was used as a background reference. For transmission electron microscopy (TEM) measurements, an aliquot of the powder was sonicated in nanopure water for 15 min. A single drop of this suspension was placed on a lacey carbon coated copper TEM grid and dried in air. The TEM examination was completed on a electron microscope operated at 200 kV to examine at electron optical magnification of 64,000 to 550,000.

**2.2.4 Photocatalytic Measurements.**

Reaction mixture preparation, photolysis conditions, and analysis procedures were similar to previous work.[64] The suspensions contained doped or undoped titania at 1.00 mg/mL. The initial concentrations of probe molecules and solution pH values were as follows: 1.0 mM **MR** at pH 8.5 ± 0.5, 0.3 mM **AN** at pH 8.5 ± 0.5, 0.15 mM quinoline at pH 6.0 ± 0.5 or pH 3.0 ± 0.5. The pH was adjusted and maintained over the photolysis by careful addition of aqueous NaOH or $HNO_3$. The solution was purged with $O_2$ and stirred in the dark for a minimum of 30 minutes before reactions. Reactions were irradiated with 350 nm broad range 4-Watt bulbs in a Rayonet minireactor or light from 75-Watt Xe arc lamp passed through a water filter and a 495 nm longpass filter. Potassium ferrioxalate was used as a chemical actinometer.[65,66] All reactions were carried out at ambient temperature with continuous stirring and $O_2$ bubbling.

For kinetics, 1 mL samples were acidified, centrifuged, filtered and analyzed by HPLC. HPLC analysis was done using a C18 reverse phase column using a diode array detector. Compounds were identified by comparison to authentic samples. **MR** degradation analysis was performed using 70% water containing 0.2% acetic acid and 30% methanol as the eluent at 1 mL/min and monitored at 290 nm. The eluent used for analysis of **AN** was 70% acetonitrile and 30% water at 1 mL/min and detected at 270 nm. Quinoline and the oxidized products were easily identifiable by HPLC. However, it was determined that using two different mobile phases was ideal for analysis of all the products, as there were some difficulties with overlap. For HPLC analysis of quinoline, 4-quinolinone

(**4HQ**), 2-aminobenzaldehyde (**2AB**), and 2-quinolinone (**4HQ**), the solvent was 1:3 methanol:water with 0.2% acetic acid. Analysis of 5-hydroxyquinoline (**5HQ**) and 8-hydroxyquinoline (**8HQ**) was done using 1:9 methanol:water with 0.2% acetic acid as the mobile phase with an elution rate of 0.75 mL/min.

For product analysis for **MR** and **AN** degradations, GC-MS (or routine GC) was used and compounds were verified by comparison to authentic samples. Approximately 60 mL of the irradiated solution was acidified, centrifuged and filtered. Fifty mL of the filtrate was concentrated by evaporation under reduced pressure until 3 – 5 mL remained, which was then freeze-dried. For GC-MS analysis of **MR** reactions, 1 mL of a 0.5 mM dodecane in pyridine stock solution was added to the residual solid followed by silylation as previously described.[61,64] For GC-MS analysis of **AN** reactions, the lyophilized solid was dissolved in 0.5 mL methanol containing 0.5 mM docecane, followed by agitation and centrifugation. GC-MS was done by GC-TOF analysis with a 30 m DB-5 column.

## 2.3 Results

### 2.3.1 Physical characterization of catalysts.

Powder diffraction data revealed that the prepared materials were anatase (Figure 1). The average particle size of S-$TiO_2$, $S_8$-$TiO_2$, and undoped $TiO_2$ were 13 nm, 13 nm, and 14 nm calculated using the Scherrer formula ($d = 0.9\lambda/\beta_{1/2}\cos\theta$). These values are consistent with the typical particle sizes of 5-15 nm observed in the transmission electron microscopy images (Figure 2). The BET surface was 93 $m^2/g$ for S-$TiO_2$ and 69 $m^2/g$ for undoped $TiO_2$.

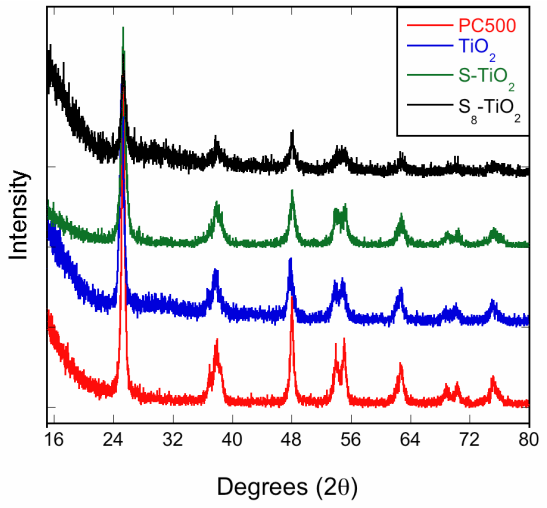


**Figure 1.** XRD of synthesized S-$TiO_2$ and $TiO_2$ compared to commercially available anatase (PC500).

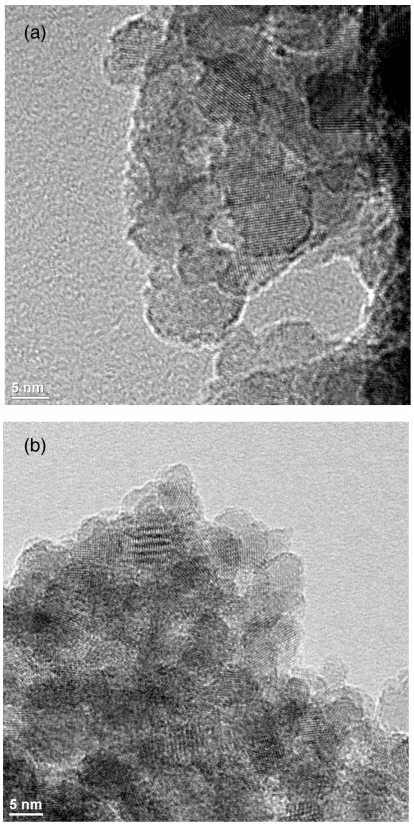


**Figure 2.** TEM images of (a) $TiO_2$ and (b) S-$TiO_2$.

Figure 3 shows the XP spectra of the S 2p region obtained under different conditions. The spectrum obtained from a dried, but un-annealed sample has a peak at 162 eV, which

corresponds to $S^{2-}$. The spectra also indicated the presence of carbon and nitrogen derived from thiourea. After annealing, the 162 eV $S^{2-}$ peak disappears and is replaced by a new one at 169 eV, indicating the presence of an $S^{4+}$ and/or $S^{6+}$ species.[67-70] Etching, which removes the first few atomic surface layers, reduced the signal strength by a factor of 2. In post-annealing spectra, no peaks corresponding to nitrogen were observed, and no carbon peaks were observed, outside of the ubiquitous carbon C 1s peak corresponding to adventitious/ambient carbon. By XPS, the total sulfur concentration was 0.8% (S-$TiO_2$) or 1.0% ($S_8$-$TiO_2$), determined before etching. In the $S_8$-$TiO_2$ sample, a small peak at 162 eV appears after etching, demonstrating the presence of $S^{2-}$. Diffuse reflectance data show that sulfur doping causes a significant red shift relative to the undoped titania prepared without the sulfur source (Figure 4).

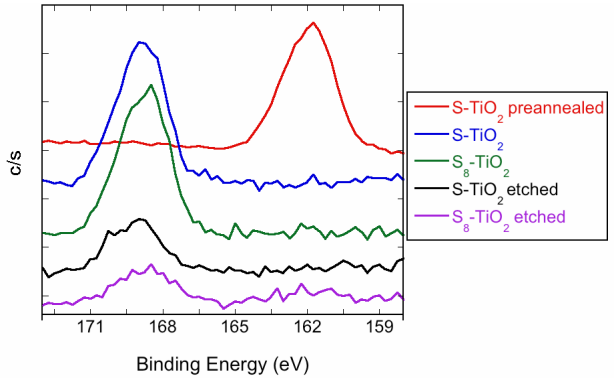


**Figure 3.** XP spectra of S-$TiO_2$.

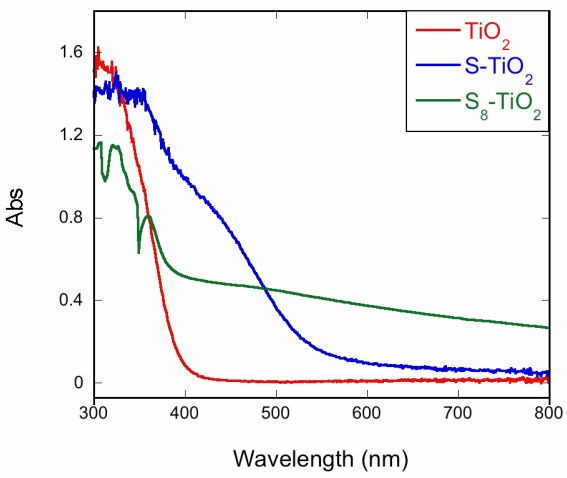


**Figure 4.** Diffuse reflectance spectra of undoped $TiO_2$ and S-$TiO_2$.

### 2.3.2 Photocatalytic Degradations.

Figure 5 shows the initial zero-order rates of loss on a logarithmic scale for photocatalytic degradation of the probe molecules. The $S_8$-TiO2 behaved very similarly to S-$TiO_2$. Control experiments showed that the organic compounds were stable under the conditions in the dark on the time scale of all reactions. Rates were normalized with actinometry from one light source to the other to account for varying photonic flux.[71] The light sources were fluorescent tubes with broad irradiation centered at 350 nm and a Xe arc lamp filtered through water (to remove excessive IR) and at 495 longpass filter. Thus, the latter is an exclusively visible (and IR) light source, while the former is fully in the UV. According to Figure 4, the undoped $TiO_2$, in the absence of any organic substrate, should not absorb any light from the >495 nm source, and such irradiation is also near the red edge of absorption for the doped catalyst. Under UV irradiation, the pristine $TiO_2$ degraded the probe molecule more rapidly than did S-$TiO_2$, by factors of approximately 2.

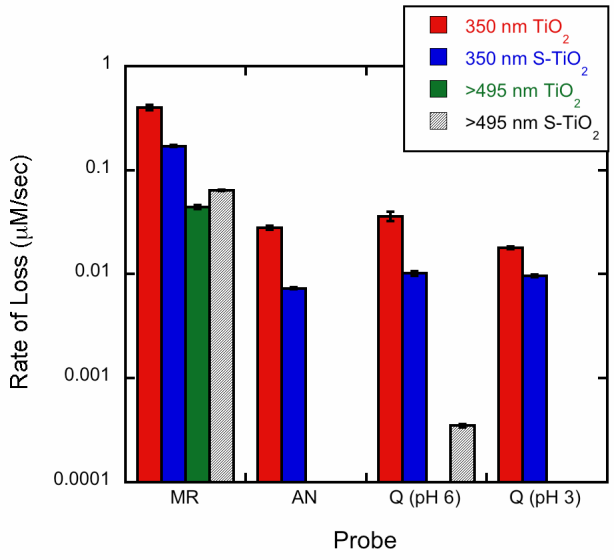


**Figure 5.** Comparison of probe molecule degradation rates for $TiO_2$ and S-$TiO_2$ photocatalytic degradation under UV and visible light. Rates are normalized for variances in light output using ferrioxolate actinometry.

**2.3.2.1 Rates of Degradation.**

**MR** was degraded faster than either of the other two probe molecules, regardless of conditions (Figure 5). Perhaps most interesting is the observation that **MR** is degraded at comparable rates when the naked catalyst does not absorb the light. Given that **MR** is an electron rich phenol, the most probably explanation is the formation of a charge transfer complex between it and $TiO_2$, which is irradiated even in the visible. The suspensions were not visibly colored, but the concentration of **MR** is sufficiently low that such obvious coloration is not expected. This type of CT complex has been documented in related molecules before.[72-74] Rates alone do not distinguish whether the >495 nm-initiated degradation with S-$TiO_2$ were based on the same CT interaction or on the visible absorption of the catalyst.

The rate of degradation of **AN** mediated by any of the catalysts under UV illumination is an order of magnitude lower than the rate of loss of **MR**. The rate for S-$TiO_2$ is smaller than that for $TiO_2$ by a factor of about 2.5, both under 350 nm irradiation. Over the course of 48 hours of irradiation (which was the practical limit for keeping the dark concentration the same within a few percent), no loss of **AN** was detectable when using >495 nm irradiation, regardless of the catalyst.

**Q** was degraded efficiently with UV light, similarly to the other two probes, at either pH 3 or 6 by both S-$TiO_2$ and $S_8$-$TiO_2$. Figure 6 shows the full set of kinetic data for degradation of **Q** using S-$TiO_2$. $S_8$-$TiO_2$ removes quinoline approximately 2.5 times faster than S-$TiO_2$ at pH 3, and 1.5 times faster at pH 6 (Figure 7). Like **AN**, loss of **Q** when using $TiO_2$ and visible irradiation was not distinguishable from the dark background. This same result was obtained when S-$TiO_2$ or $S_8$-$TiO_2$ was used as the photocatalyst at pH 3 under >495 nm irradiation. However, at pH 6, **Q** was reproducibly degraded at a normalized rate about two orders of magnitude more slowly than under UV irradiation (15% in 48 hours) by S-$TiO_2$ and wavelengths >495 nm. However, since the fraction of absorbed photons is not known, but is very likely lower for the visible

irradiations, this should be taken as a lower limit of the relative rates and not an absolute ratio.

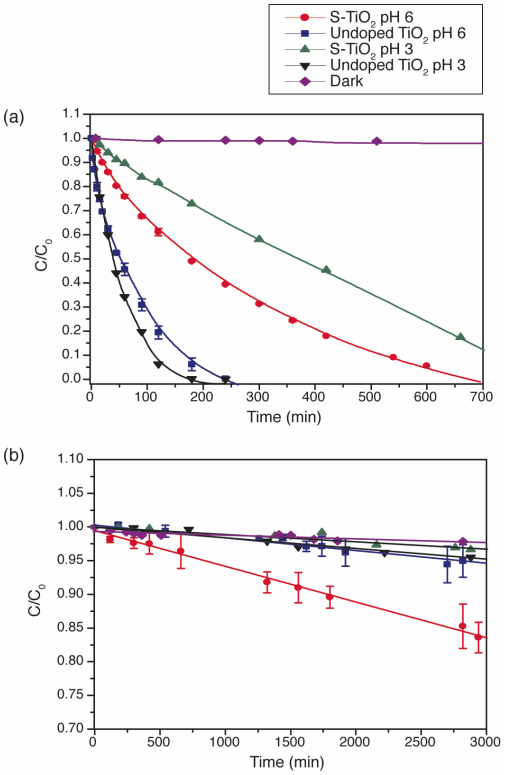


**Figure 6.** Heterogeneous photocatalytic degradation of quinoline under (a) 350 nm and (b) ≥495 nm.

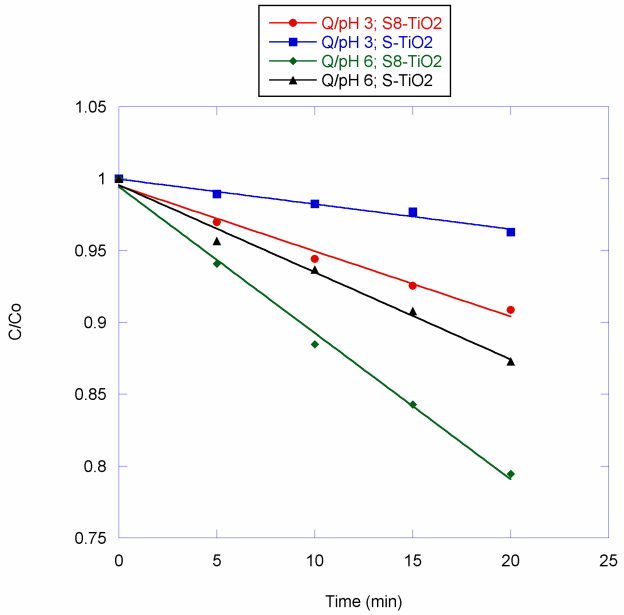


**Figure 7.** Initial kinetics of degradation of quinoline under 350 nm irradiation by $S_8$-$TiO_2$ and S-$TiO_2$.

### 2.3.2.2 Product Analysis.

Product analysis at fixed low conversion can provide useful, if qualitative, information about the relative rates of formation of initial degradation products. The major concern is the secondary consumption of the intermediates; in extreme cases, no intermediates are observed at all because they are consumed much more rapidly than they are formed. However, the present compounds were chosen in large part because their early degradation products are observable and chemically interpretable. An admittedly simplified scheme for each molecule, based on previous studies, is given in Scheme 1. A few of these products clearly require more than one step (e.g., **MBA**, which is undoubtedly secondary to **MB**). Hydroxymethoxy hydroquinone (**HMH**) spontaneously oxidizes to the quinone in aerated water on handling, although the reverse reaction[75] almost certainly takes place with the light on.

Table 1 summarizes the results of product studies for all the probes and catalysts for low conversion, with the products grouped together as indicating hydroxyl-like chemistry or SET-initiated chemistry, as indicated in Scheme 1. The ratios given in Table 1 for **MR**

show there is a slight excess of SET products over $HO\bullet_{ads}$ products, but both pathways are competitive. Moving from UV to visible, the product yield shifts for $TiO_2$, but does not do so for S-$TiO_2$.

**Table 1.** Ratios of early degradation intermediate products.

| | Observed SET:$HO\bullet_{ads}$ intermediate product ratio[a] | | | |
|---|---|---|---|---|
| | $TiO_2$ | | S-$TiO_2$ | |
| Probe molecule | UV | Visible | UV | Visible |
| 4-methoxyresorcinol, **MR**[b] | 1.3 | 1.7 | 1.2 | 1.2 |
| *p*-anisyl-1-neopentanol, **AN**[b] | 0.9[c] | -- | 0.1 | -- |
| quinoline, **Q** (pH 6) | 4.2 | -- | 6.2 | SET only |
| quinoline, **Q** (pH 3) | 0.2[d] | --[d] | 0.04 | --[d] |

[a]**MR** and **AN** product ratios where found using GC peak areas relative to dodecane as an internal standard. **Q** product ratios were found by concentrations based on HPLC peak areas versus standard calibrations. [b]pH 8.5 ± 0.5. [c]Peak areas in the GC trace were very small, indicating intermediate products may be consumed faster than the parent probe molecule. [d]Trace amounts of 5HQ were observed.

For **AN**, no products were observed for the visible irradiations, as indicated by the kinetics experiments. For this poorly binding substrate, when UV irradiation at pH 8.5 was used, hydroxyl products predominate only slightly in the undoped $TiO_2$, but quite strongly when S-$TiO_2$ is the catalyst. (This latter result was also our observation using commercially available anatase catalysts[62].) The product peaks were smaller than expected, implying that even at modest degradation of the parent compound, secondary degradation reactions were important. This phenomenon is not particularly surprising for poorly binding substrates; the more oxidized products may more easily be adsorbed to the catalyst.

Degradations were carried out at pH 3 and 6 for quinoline, which is below and above the pKa of quinolinium ion, respectively. Traces showing the product evolution as a function of irradiation time for quinoline, using $TiO_2$ as the catalyst, are given in Figure 8. Figure 9 shows the same data for quinoline and S-$TiO_2$, including the > 495 nm photolyses. $S_8$-$TiO_2$ behaved in the same manner as S-$TiO_2$ in >495 nm degradations of quinoline at both pH 3 and 6.

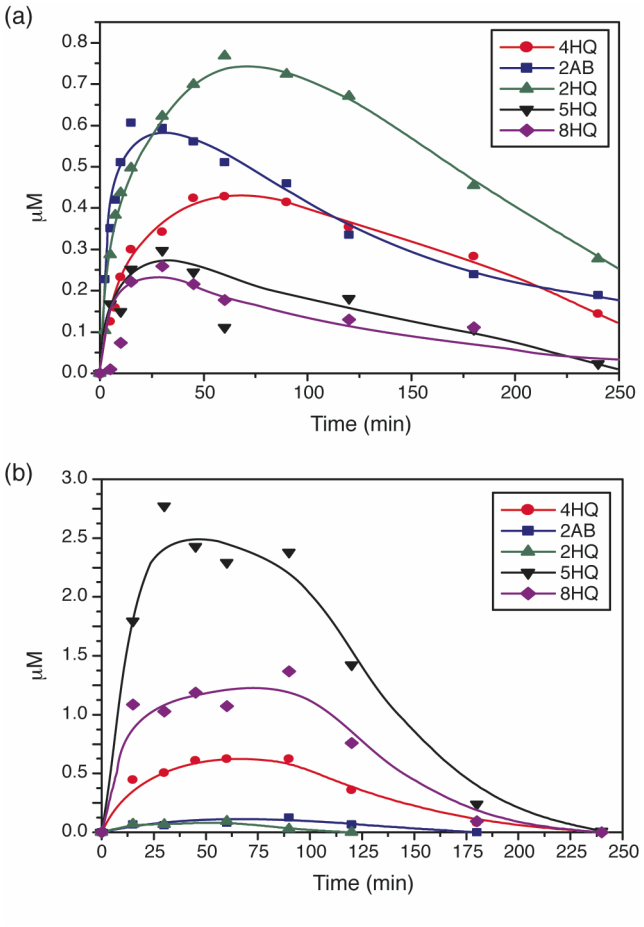


**Figure 8.** Intermediate products formed from the $TiO_2$-mediated degradation of quinoline at (a) pH 6 and (b) pH 3.

With UV exposure, the SET products were favored by a slightly larger margin with the sulfur-doped catalyst, compared to the undoped. A dramatic difference in the absolute ratio is seen for the quinoline (pH 6) vs. quinolinium (pH 3) case (Figures 8 and 9). Intermediate product studies after two hours reveal that $S_8$-$TiO_2$ favored SET products by

more than 10:1 at pH 6 and hydroxyl products by more than 23:1 at pH 3. In general, the favoring of SET products at pH 6 is very likely due to superior adsorption of the neutral compound through the nitrogen lone pair, favoring SET as a mechanism[11].

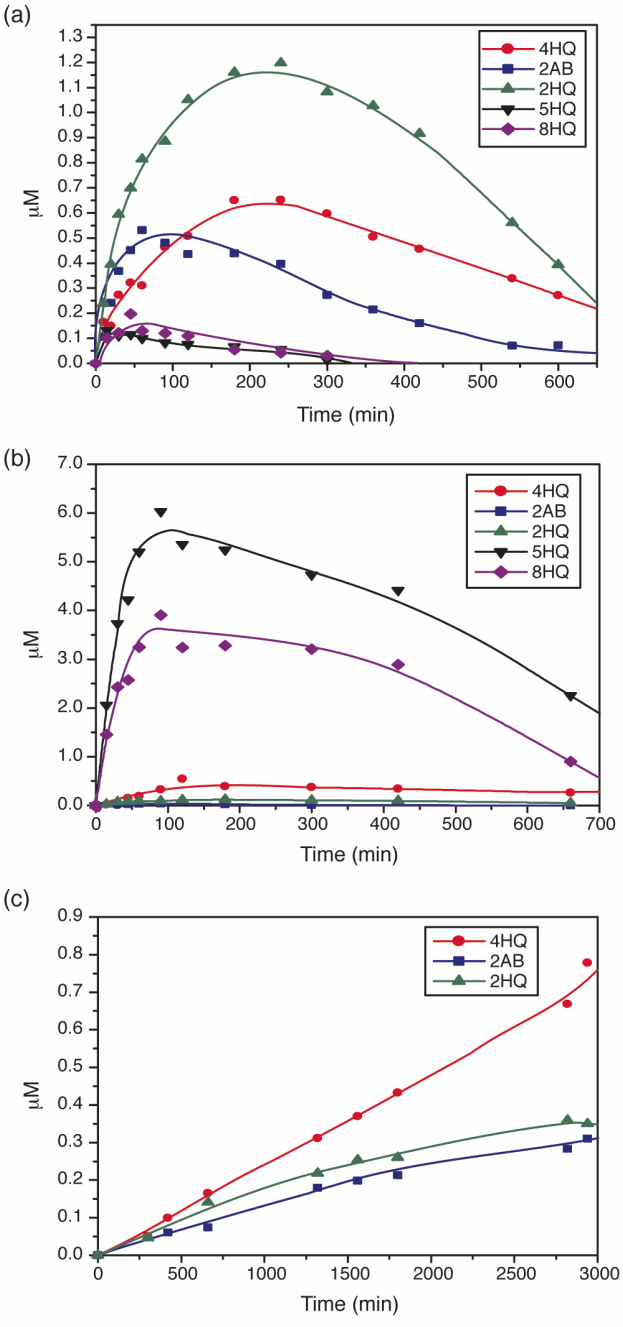


**Figure 9.** Intermediate products formed from the S-$TiO_2$-mediated degradation of quinoline at (a) pH 6 under 350 nm photolysis, (b) pH 3 under 350 nm photolysis, and (c) pH 6 under ≥495 nm.

These results are consistent with those obtained by the Pichat group using P25 as the photocatalyst[11]. However, Pichat reports **2AB** as the major product, in contrast to the current observations. We were able to reproduce the Pichat result by using P25 as a photocatalyst instead of the pure anatase used in this study. Thus the internal change within the SET product distribution is attributable to differences in the catalyst.

With visible photolysis of **Q**, there was a dramatic difference between the catalysts, as noted by the kinetics experiments as well. The undoped $TiO_2$ did not catalyze any degradation as detected by kinetics at pH 6, but S-$TiO_2$ did, with the products being entirely SET-derived. Despite the loss of **Q** being indistinguishable from dark reaction at pH 3, trace amounts of **5HQ** could be detected.

Additional control experiments were done to determine if slightly higher energy visible light could be used to generate hydroxyl chemistry. Quinolinium degradation at pH 3 was the probe of choice for this. Instead of using 495 nm cutoff filters, two sets of otherwise identical experiments were carried out at pH 3, using 435 nm and 455 nm cutoff filters respectively. As shown in Figure 4, these cutoff wavelengths are both longer than the classical absorption of the $TiO_2$. Also, as a negative control, undoped $TiO_2$ was examined under the same conditions. The results for all three cutoffs (435 nm, 455 nm, and 495 nm) were the same within experimental uncertainty, i.e., no hydroxyl-mediated degradation.

## 2.4 Discussion

### 2.4.1 Catalyst physical properties.

The method of doping $TiO_2$ with thiourea, as per Ohno's procedure is now well established and reproducible. Thiourea is a good source of nucleophilic sulfur; in organic synthesis, it is used as a synthon for $HS^-$. (After initial reaction with an electrophile, a second step is usually used to hydrolyze the initial adduct and give urea as a byproduct.) To that extent, it is a sensible source of S for sol-gel preparations of $TiO_2$. XPS data

obtained before annealing (showing $S^{2-}$) are consistent with either thiourea as a physical mixture with the titania or with a covalent modification in which the oxidation state of sulfur has not changed. High temperature annealing under $O_2$ is necessarily oxidative, however, and $S^{4+}$ and/or $S^{6+}$ are what is observed thereafter. Since C and N are not detected by XPS, it is presumed that these are largely "burned off" by the high temperature annealing {NOTE: Small amounts of "atmospheric" carbon are always detected by XPS; we cannot eliminate the possibility of small amounts of graphitic type carbon in the final catalyst.}. Indeed, Jin and coworkers showed through DSC measurements on similar preparations, that there is an exotherm near 220 ˚C attributable to decomposition of urea/thiourea, and others near 265 ˚C and 430˚C attributed to combustion of other organic substances[22]. It is also during the annealing process that the yellow color of the catalyst is developed, clearly indicating chemical incorporation of the S at this stage. The post-annealing spectra correspond to the sulfate oxidation state (or potentially $SO_2$), and suggest S-for-Ti substitution, as proposed by Ohno[36,45]. The etched XPS spectra show that the sulfur goes down at least several layers, though we presume it to be dispersed throughout.

The $S_8$-$TiO_2$ showed the same XPS data, save for a small $S^{2-}$ peak after etching, which could suggest a minor fraction of S-for-O substitution. As with the Ohno-style, S-$TiO_2$, there could be a small amount of carbon also included, because of small amounts of residual solvent that remain after drying. This is difficult to be certain of because the XPS for adventitious carbon adsorbed to the material from air overlaps strongly with the most likely resulting carbon product, i.e., coke condensation. The mechanism for incorporation of S in this material is uncertain. At this high temperature, initiation of sulfur chemistry by both homolysis and nucleophilic type attack is reasonable. The fact that the S remains in the XPS spectra after Ar-etching does imply that significant rearrangement of the surfaces and nearby layers occurs at this temperature, in that "penetration" of the sulfur in the $TiO_2$ is required by this result. Since the material generated by annealing with $S_8$ appears to be functionally equivalent to that generated by preparation with thiourea, it would seem there are advantages to preparing sulfur-doped

$TiO_2$ in this manner: better optimization of the initial $TiO_2$ manufacture, and lower expense of the dopant. Optimization of the annealing step and/or use of other titania samples (e.g., P25) may result in a superior catalyst.

**2.4.2 Photocatalytic results.**

The specifics of the oxidations of these three compounds, of course, are much less valuable than the generalities that can be drawn from them; these results must be placed in the context of various other types of physical studies, and we review the available literature to put the current results in context. At least for this set of probes, a consistent result was that degradation using UV light was slowed by the sulfur doping. This is similar to the observations of Sun, who also found an inverse relationship between activity in the visible and UV for C- and S- doped $TiO_2$[22].

Apparently, contradictory arguments are made by various authors for the chemistry that should be derived from doped $TiO_2$. These are manifest both in the explanation of kinetics and for the reactivity of the photogenerated holes. Consider, for example, the current observation that, under UV photolysis, S-$TiO_2$ always provided slower degradations than did $TiO_2$.

Sun attributed the lower UV activity to S centers acting as recombination sites[22]. On the other hand, Tachikawa, based on flash photolysis experiments, concluded that S sites did not act as recombination centers[47]. By time-resolved diffuse reflectance spectroscopy (in acetonitrile or methanol), Majima and coworkers determined that the yield of charge carriers with 355 nm excitation is greater for undoped $TiO_2$ than for S-$TiO_2$ (made by the sol gel method with thiourea). However, the efficiency of hole transport to the surface is comparable for the two materials and the S-centers do not act as special recombination points[47]. The lower total number of charge separations naturally leads to a lower observed rate of disappearance.

On the other hand, mainly on the basis of efficiency measurements over a series of catalysts, Jin and coworkers conclude quite the opposite. They argue that the sulfur defects do act as recombination centers, and it is by this means that the UV efficiency is slightly lowered[22]. The current results do not settle this particular dispute. Instead, they reinforce the observation that this effect, that UV photocatalytic efficiency for the S-doped materials should be expected to be universally lowered, relative to the undoped case.

Thus, from a practical standpoint of optimizing a catalyst, the advantage or disadvantage of S-$TiO_2$ (in terms of speed of degradation) will depend entirely on the spectral distribution of the light source being used and the transmission of that light to the catalyst. The advantage of activity in the visible would have to make up for the loss of activity in the UV.

Therefore, to understand whether S-$TiO_2$ is an "improvement" over $TiO_2$, knowing how universal and efficient the degradation initiated by visible irradiation is critical. If only certain substrates will be oxidized, and others untouched, its utility would certainly be limited to niche applications.

Given the model that main group dopants provide mid-gap filled orbitals, rather than changing the band structure of $TiO_2$ in a more fundamental way, an intuitive argument can be made that the S-centers represent "deep" $h^+$ traps, i.e., high energy orbitals from which electrons may fall. This should inherently lower the oxidizing power of the hole, relative to undoped $TiO_2$ assuming charge migration is faster than reaction with the organic substrate. The consequences of the "deep hole trapping", however, remain a matter of discussion.

Majima and coworkers give a report that would be pessimistic regarding visible activity of their S-$TiO_2$ (also made by the Ohno method), at least in organic solvents. With 430 nm excitation, these authors report the formation of charge carriers, and formation of

organic radical cations by direct irradiation of CT bands, but no SET oxidation of the organic adsorbate 4-(methylthio)benzyl alcohol after excitation[47].

Takeshita and coworkers contrasted the behavior of S-$TiO_2$ made by oxidative annealing of $TiS_2$ and by the Ohno method with thiourea[57]. Essential to their analysis was the observation that the sulfur remaining in the $TiS_2$-based catalyst was largely in the center of the particle, with very little remaining in the exterior. This is in contrast to the sol-gel method, assumed to produce approximately homogeneously dispersed S. They argue, on the basis of flash photolysis experiments, that the sol-gel materials produce near-surface holes that are not capable of oxidizing water to produce HO•, but are able to oxidize methanol[57]. (This occurs whatever the excitation wavelength.) With the $TiS_2$-based material, visible irradiation does not produce photoactivity, which is rationalized by assuming that the sulfur centers are deep within the particle and the charge carriers cannot migrate to the surface.

By contrast, for carbon-doped $TiO_2$, Nakato reports that visible photooxidation of methanol goes by an indirect oxidation pathway functionally equivalent to $HO•_{ads}$ chemistry. This conclusion is based upon measurement of photocurrent in the presence and absence of methanol. Although the catalyst is not identical to the present case, the authors discuss the generality of this mechanism[13]. The chemical contrast, in that case, is that hydrogen abstraction of the C-H is the first step of methanol oxidation, rather than SET, followed by deprotonation, current doubling, and so on. In principle, this might be distinguished by means of competition experiments with isotope labeling, where the hydrogen abstraction should show a kinetic isotope effect.

Our method, instead, depends on a different chemical outcome by the two mechanisms, and indirect reasoning about the physical processes. The three probes used here each demonstrate a different pattern of reactivity, but can be assembled into a sensible whole.

#### 2.4.2.1 Photocatalytic degradation of MR.

The pH of 8.5 was chosen to study the "remediation" of **MR** because this was the pH at which degradation was the most efficient, and intermediates from both SET and hydroxyl chemistry had been observed[61]. Indeed, **MR** was degraded under these conditions more rapidly than either of the other probes. This is presumably attributable to both stronger adsorption[62] and a lower oxidation potential, though reversible oxidation potentials are not available for these compounds.

The most important result with **MR**, however, was the observation of both major oxidation pathways, even with visible light well to the red of the absorbance cutoff of $TiO_2$. The chemistry occurring here could not result from the direct excitation of the undoped $TiO_2$ semiconductor since the light used here does not possess enough energy. We attribute this reactivity to the formation and direct irradiation of a charge transfer (CT) complex, which has been directly observed between phenol compounds and $TiO_2$[72-74,77]. Although the intuitive expectation is for CT irradiation to result in chemistry essentially identical to normal SET chemistry, the work of Agrios and Gray show wavelength dependence and multiple types of reactivity[73,74]. Indeed, we report a closely related phenomenon in Table 1, where the product ratios differ for the doped and undoped catalyst, presumably because some of the irradiation is direct to the catalyst in the case of S-$TiO_2$. Although interesting as an independent phenomenon, this CT-based degradation does not significantly bear on whether S-$TiO_2$ will be a broadly useful catalyst, since only a subset of pollutants will form such CT complexes.

#### 2.4.2.2 Photocatalytic degradation of AN.

The degradation of **AN** with the Millenium Chemicals PC series, reported on previously[62], showed hydroxyl products dominating at neutral and higher pH. This is similar to the result reported for S-$TiO_2$ and UV irradiation in Table 1, but the total amount of observed intermediates was very small, in contrast, for undoped $TiO_2$. The smaller quantities are consistent with secondary degradation that is faster than the first step.

Loss of **AN** mediated by either S-$TiO_2$ or $TiO_2$ with > 495 nm light was insignificant. While this is the expected result for $TiO_2$, the S-$TiO_2$ shows modest absorption in this region and should be capable of generating charge carriers (and apparently does, given the results for quinoline). The lack of degradation of this molecule is thus reasonably damning to the prospects of S-$TiO_2$ as a versatile visible-light driven catalyst, at least this far into the visible. At least for this compound, both the SET and hydroxyl-like chemistry are shut down in the visible. The SET chemistry might be expected to be molecule-specific, i.e., that some more easily oxidized or better binding molecules might undergo SET even with the "weaker" holes due to the doping. However, though some controversy exists over the exact nature of the hydroxyl-like chemistry, it is widely believed to be "indirect", in that an intermediate (TiO•, HO•, etc.) is produced that in turn reacts with the substrate. As **AN** is dominated by this chemistry in the UV, the lack of degradation of **AN** with lower energy light is strongly suggestive that the indirect oxidizing center is not formed.

**2.4.2.3 Photocatalytic degradation of Q.**

The last probe, quinoline, leads to a variety of products under photocatalytic conditions, as a result of electronic demand differences in the benzene and pyridine rings. Pichat and coworkers showed that electrophilic hydroxyl radicals (e.g., Fenton conditions) favor addition to the benzene ring, and SET chemistry favors functionalization of the pyridine ring and formation of **2AB** and **4HQ**[11]. The product distribution results reported here follow the trends of Pichat and coworkers, save for the differences in internal ratios of SET products, but as noted, we were able to reproduce their results when using the same catalyst they did, i.e., P25.

Above the pKa of quinolinium, it is assumed that adsorption to the catalyst occurs largely through the nitrogen lone pair. At low pH, quinolinium is predominant and not as likely to adsorb to the also-positively-charged $TiO_2$ surface[78]. Not only does the poor binding suppress SET chemistry, but the protonation obviously increases the oxidation potential. We suggest that the approximate invariance in rate of degradation of **Q** with pH (Figures 5, 6) is merely coincidence.

Like **AN**, quinoline does not form a CT complex with $TiO_2$ that is degraded on visible excitation above the dark baseline, though trace **5HQ** is observed at pH 3. (We presume that this is diagnostic of a very minor amount of hydroxyl chemistry that was simply undetected in the **AN** case.) Both **5HQ** and **8HQ** were observed with UV irradiation and $TiO_2$ (Figure 8).

However, with S-$TiO_2$, **Q** is significantly degraded by visible light at pH 6, if only through the SET pathways. Only SET products **2AB**, **2HQ**, and **4HQ** (Figure 9) are observed. We infer that the reactive holes in S-$TiO_2$ are able to oxidize quinoline, even if they are not able to do the same for **AN**.

## 2.5 Conclusion

Information on the mechanistic differences between S-$TiO_2$ and undoped $TiO_2$ was obtained through the use of three probe molecules. **MR**, **AN**, and **Q** each showed a different pattern of reactivity with respect to visible irradiation, with activity from both catalysts, neither catalyst, and only S-$TiO_2$, respectively. The simplest interpretation of the results presented here is that S-$TiO_2$, prepared by the Ohno method, does not produce active hydroxyl-like sites on excitation at > 495 nm. Furthermore, the sulfur doping sites do act as deep hole traps that diminish the oxidizing power of the hole. Moreover, we observe, consistent with previous workers, that the UV activity of S-$TiO_2$ is somewhat diminished from its parent. As a result, the utility of S-$TiO_2$ over a broadly useful $TiO_2$ catalyst such as P25 will come when extension of the absorption spectrum into the visible is more important than efficient use of UV photons, and when the target pollutants are relatively easy to oxidize. It is generally the case that the early degradation steps – at least of aromatic type pollutants – make the resulting compounds easier to degrade by photocatalysis, so this latter restriction may not be as daunting as it might seem at first glance. It may also be useful as a component of a catalyst mixture designed to efficiently use the UV and also derive some activity from visible irradiation. Finally, due to the very similar results obtained for S-$TiO_2$ and $S_8$-$TiO_2$ (without significant optimization of the

$S_8$ annealing step), and the ease of preparation and low cost of the sulfur atoms, the approach of annealing $S_8$ into extant $TiO_2$ catalysts (e.g., P25) may turn out to be an attractive approach.

## 2.6 References

(1) Pichat, P. *Water Sci. Technol.* **2007**, *55*, 167-173.

(2) Ryu, J.; Choi, W. *Environ. Sci. Technol.* **2008**, *42*, 294-300.

(3) Ollis, D.F.; Al-Ektabi, H, Eds. *Photocatalytic Purification and Treatment of Water and Air;* Elsevier Science Publishers: New York, 1993.

(4) Hoffmann, M.R.; Martin, S.T.; Choi, W.; Bahnemann, D.W. *Chem. Rev.* **1995**, *95*, 69-96.

(5) Robertson, P.K.J.; Bahnemann, D.W.; Robertson, J.M.C.; Wood, F.; *Handbook of Envrionmental Chemistry*, **2005**, *2*, 367-423.

(6) Fujishima, A.; Zhang, X.; Tryk, D.A. *Surface Science Reports*, **2008**, *63*, 515-582.

(7) Thompson, T.L.; Yates, J.T. *Chem. Rev.* **2006**, *106*, 4428-4453.

(8) Fox, M.A.; Dulay, M.T. *Chem. Rev.*, **1993**, *93*, 341-357.

(9) Linsebigler, A.L.; Lu, G.; Yates, Jr. J.T. *Chem. Rev.* **1995**, *95*, 735-758.

(10) Legrini, O.; Oliveros, E.; Braun, A.M.; *Chem. Rev.* **1993**, *93*, 671-698.

(11) Cermenati, L.; Pichat, P.; Guillard, C.; Albini, A. *J. Phys. Chem. B.* **1997**, *101*, 2650-2658.

(12) Park, J.S.; Choi, W. *Chem. Lett.* **2005**, *34*, 1630-1631.

(13) Liu, H.; Imanishi, A.; Nakato, Y. *J. Phys. Chem. C.* **2007**, *111*, 8603-8610.

(14) Asahi, R.; Morikawa, T.; Ohwaki, T.; Aoki, K.; Taga, Y. *Science* **2001**, *293*, 269-271.

(15) Anpo, M. *Catal. Surv. Jpn.* **1997**, *1*, 169-179.

(16) Choi, W.; Termin, A.; Hoffmann, M.R. *J. Phys. Chem.* **1994**, *98*, 13669-13679.

(17) Umebayashi, T.; Yamaki, T.; Tanaka, S.; Asai, K. *Chem. Lett.* **2003**, *32*, 330-331.

(18) Wang, H.; Lewis, J.P.; *J. Phys.: Condens. Matter* **2005**, *17*, L209-L213.

(19) Wang, H.; Lewis, J.P.; *J. Phys.: Condens. Matter* **2006**, *18*, 421-434

(20) Wang, X.; Meng, S.; Zhang, X.; Wang, H.; Zhong, W.; Du, Q. *Chem. Phys. Lett.* **2007**, *444*, 292-296.

(21) Choi, Y.; Umebayashi, T.; Yoshikawa, M. *J. Mater. Sci.* **2004**, *39*, 1837-1839.

(22) Sun, H.; Bai, Y.; Cheng, Y.; Jin, W.; Xu, N. *Ind. Eng. Chem. Res.* **2006**, *45*, 4971-4976.

(23) Chen, Z.; Yu, G.; Zhang, P.; Jiang, Z. *Huanjing Kexue*, **2002**, *23*, 55-59.

(24) Chen, X.; Burda, C. *J. Phys. Chem. B.* **2004**, *108*, 15446-15449.

(25) Chen, D.; Jiang, Z.; Geng, J.; Wang, Q.; Yang, D. *Ind. Eng. Chem. Res.* **2007**, *46*, 2741-2746.

(26) Irie, H.; Watanabe, Y.; Hashimoto, K. *Chem. Lett.* **2003,** *32*, 772-773.

(27) Irie, H.; Watanabe, Y.; Hashimoto, K. *J. Phys. Chem. B.* **2003,** *107*, 5483-5486.

(28) Irie, H.; Watanabe, Y.; Hashimoto, K. *Chem. Lett.* **2003,** *32*, 772-773.

(29) Li, Y.; Hwang, D.-S.; Lee, N.H.; Kim, S.-J. *Chem. Phys. Lett.* **2005**, *404*, 25-29.

(30) Yang, J.; Bai, H.; Tan, X.; Lian, J. *Applied Surface Science*, **2006**, *253*, 1998-1994.

(31) Yang, K.; Dai, Y.; Huang, B. *J. Phys. Chem. C.* **2007**, *111*, 12086-12090.

(32) Sakthivel, S.; Kisch, H. *Angew. Chem. Int. Ed.* **2003**, *42*, 4908-4911.

(33) Sakthivel, S.; Janczarek, M.; Kisch, H. *J. Phys. Chem. B.* **2004**, *108*, 19384-19387.

(34) Xu, C.; Killmeyer, R.; Gray, M.L.; Khan, S.U.M. *Appl. Catal. B.* **2006**, *64*, 312-317.

(35) Xu, T.-H.; Song, C.-L.; Liu, Y.; Han, G.-R. *J. Zhejiang Univ. Sci. B.* **2006**, *7*, 299-303.

(36) Ohno, T.; Akiyoshi, M.; Umebayashi, T.; Asai, K.; Mitsui, T.; Matsumura, M. *Appl. Catal. A.* **2004**, *265*, 115-121.

(37) Ohno, T.; Tsubota, T.; Nishijima, K.; Miyamoto, Z. *Chem. Lett.* **2004**, *33*, 750-751.

(38) Reddy, K.M.; Baruwati, B.; Jayalakshmi, M.; Rao, M.M.; Manorama, S.V. *J. Solid State Chem.* **2005**, *178*, 3352-3358.

(39) Zhang, Q.; Wang, J.; Yin, S.; Sato, T.; Saito, F. *J. Am. Ceram. Soc.*, **2004**, *87*, 1161-1163.

(40) Umebayashi, T.; Yamaki, T.; Itoh, H.; Asai, K. *Appl. Phys. Lett.* **2002,** *81***,** 454-456**.**

(41) Hamal, D.B.; Klabunde, K.J. *Journal of Colloid and Interface Science*, **2007**, *311*, 514-522.

(42) Katoh, M.; Aihara, H.; Horikawa, T.; Tomida, T. *J. Coll. Interf. Sci.* **2006**, *298*, 805-809.

(43) Ho, W.; Yu, J.C.; Lee, S. *J. Solid State Chem.* **2006**, *179*, 1171-1176.

(44) Ohno, T.; Mitsui, T.; Matsumura, M. *Chem. Lett.* **2003**, *32*, 364-365.

(45) Ohno, T.; Tsubota, T.; Toyofuku, M.; Inaba, R. *Catal. Lett.* **2004**, *98*, 255-258.

(46) Yan, X.; Ohno, T.; Nishijima, K.; Abe, R.; Ohtani, B. *Chem. Phys. Lett.* **2006**, *429*, 606-610.

(47) Tachikawa, T.; Tojo, S.; Kawai, K.; Endo, M.; Fujitsuka, M.; Ohno, T.; Nishijima, K.; Miyamoto, Z.; Majima, T. *J. Phys. Chem. B.* **2004**, *108*, 19299-19306.

(48) Liu, S.; Chen, X. *J. Haz. Mat.* **2008**, *152*, 48-55.

(49) Crisan, M.; Braileanu, A.; Raileanu, M.; Zaharescu, M.; Crisan, D.; Dragan, N.; Anastasescu, M.; Iancucescu, A.; Nitoi, I.; Marinescu, V.E.; Hodoregea, S.M. *Journal of Non-Crystalline Solids* **2008**, *354*, 705-711.

(50) Yin, S.; Komatsu, M.; Zhang, Q.-W.; Li, R.-X..; Tang, Q.; Saito, F.; Sato, T. *Guocheng Gongcheng Xuebao* **2006**, *6*, 477-481.

(51) Zhou, Z.; Xhang, X.; Wu, Z.; Dong, L. *Chinese Science Bulletin* **2005**, *50*, 2691-2695.

(52) Li, H.; Zhang, X.; Huo, Y.; Zhu, J. *Environ. Sci. Technol.* **2007**, *41*, 4410-4414.

(53) Tian, F.; Liu, C. *J. Phys. Chem. B.* **2006**, *110*, 17866-17871.

(54) DiValentin, C.; Pacchioni, G.; Selloni, A. *Chem. Mater.* **2005**, *17*, 6656-6665.

(55) Tachikawa, T.; Takai, Y.; Toji, S.; Fujitsuka, M.; Irie, H.; Hashimoto, K.; Majima, T. *J. Phys. Chem. B.* **2006**, *110*, 13158-13165.

(56) Kuznetsov, V.N.; Serpone, N. *J. Phys. Chem. B.* **2006**, *110*, 25203-25209.

(57) Takeshita, K.; Yamakata, A.; Ishibashi, T.; Onishi, H.; Nishijima, K.; Ohno, T. *J. Photochem. Photobiol. A.:Chem.* **2006,** *177*, 269-275.

(58) Tschirch, J.; Bahnemann. D.; Wark, M.; Rathousky, J. *J. Photochem. Photobiol. A.* **2008,** *194*, 181-188.

(59) Tschirch. J.; Dillert, R.; Bahnemann. D.; Proft, B.; Bierdermann, A.; Goer, B. *REs. Chem. Int.* **2008**, *34*, 381-392.

(60) Ranchella, M.; Rol, C.; Sebastiani, G.V. *J. Chem. Soc. Perkin Trans.* **2000**, *2*, 311-315.

(61) Li, X.; Cubbage, J.W.; Jenks, W.S. *J. Photochem. Photobiol. A.* **2001**, *143*, 69-85.

(62) Hathway, T.; Jenks, W.S. *J. Photochem. Photobiol. A.* **2008,** *200*, 216-224.

(63) Lang'at-Thoruwa, C.; Song Tong, T.; Hu, J.; Simons Andrean, L.; Murphy Patricia, A. *J. Nat. Prod.* **2003**, *66*, 149-151.

(64) Li, X.; Cubbage, J.W.; Tetzlaff, T.A.; Jenks, W.S. *J. Org. Chem.* **1999**, *64*, 8509-8524.

(65) Bowman, W.D.; Demas, J.N. *J. Phys. Chem.* **1976**, *80*, 2434-2435.

(66) Hatchard, C.G.; Parker, C.A. *Proc. Royal Soc. A.* **1956**, *235*, 518-536.

(67) Moulder, J.F.; Stickle, W.F., Sobol, P.E.; Bomben, K.D. *Handbook of X-Ray Photoelectron Spectroscopy*; Perkin-Elmer Corporation (Physical Electronics): Eden Prairie, MN: 1992.

(68) Sayago, D.I.; Serrano, P.; Bohme, O.; Goldoni, A.; Paolucci, G.; Roman, E.; Martin-Gago, J.A. *Phys. Rev. B.* **2001**, *64*, 205402/1-205402/7.

(69) Sayago, D.I.; Serrano, P.; Bohme, O.; Goldoni, A.; Paolucci, G.; Roman, E.; Martin-Gago, J.A. *Surface Science.* **2001**, *482-485*, 9-14.

(70) Roman, E.; De Segovia, J.L.; Martin-Gago, J.A.; Comtet, G.; Hellner, L. *Vacuum* **1997**, *48*, 597-600.

(71) The rates are not quantum yields; no attempt was made to quantify the fraction of light absorbed.

(72) Kim, S.; Choi, W. *J. Phys. Chem. B.* **2005**, *109*, 5143-5149.

(73) Agrios, A.G.; Gray, K.A.; Weitz, E. *Langmuir*, **2003**, *19*, 5178.

(74) Agrios, A.G.; Gray, K.A.; Weitz, E. *Langmuir*, **2004**, *20*, 5911-5917.

(75) Richard, C. *New J. Chem.* **1994**, *18*, 443-445.

(76) Small amounts of "atmospheric" carbon are always detected by XPS; we cannot eliminate the possibility of small amounts of graphitic type carbon in the final catalyst.

(77) Orlov, A.; Watson, D.J.; William, F.J.; Tikhov, M.; Lambert, R.M. *Langmuir*, **2007**, *23*, 9551-9554.

(78) Due to analytical difficulties the Pichat group was unable to quantify 8HQ, but we were able to separate this material chromatographically from the others.

# Chapter 3

# $WO_3$ and WC-$WO_3$-Mediated Photocatalytic Degradations of Quinoline

## 3.1 Introduction and Previous Studies

The photocatalytic activity of various metal oxide semiconductors has been thoroughly studied.[1] Currently, titanium dioxide and modified titanium dioxides have been shown to have the highest photocatalytic activity, and have been used for air purification and self-cleaning building materials,[1-3] among other practical uses. Tungsten trioxide is also an n-type semiconductor photocatalyst like titanium dioxide, but has been shown to have low activity for the degradation of organic compounds in previous studies.[4] For a semiconductor to be a successful photocatalyst, the conduction band level should be more negative than the potential for single-electron reduction of oxygen in order for the photoexcited electrons to be consumed by molecular oxygen. The consumption of photogenerated electrons is necessary to prevent charge carrier recombination and allow the photogenerated valence band holes to oxidize organic molecules. It is thought that tungsten trioxide is a not a suitable photocatalyst because of the potential of the bottom of the conduction band [+0.4 V vs. normal hydrogen electrode (NHE) at pH=0], thus electrons cannot be consumed through a one electron reduction of molecular oxygen [$O_2 + e^- + H^+ \rightarrow HO_2$, $E^0$=-0.046 V vs. NHE at pH=0].[5] Trapping of photogenerated electrons is necessary for the valence band holes to be available to oxidize organic molecules instead of being consumed in a recombination reaction; molecular oxygen is usually used as an electron trap. It is thought that $WO_3$ can only act as an effective photocatalyst when a strong electron acceptor, such as $Ag^+$ (as an alternative to $O_2$) is present.[6] Gerischer and coworkers have proposed that the rate of photooxidation of organic molecules on a catalyst surface is limited by the rate of electron transfer to oxygen.[7,8,9]

### 3.1.1 Pt-$WO_3$

An understanding of Pt-$WO_3$ systems is a good starting point for the study of WC-$WO_3$ and $WO_3$ photocatalysts. Platinum is a heavily studied dopant and WC is thought to be a

less expensive, but electrochemically similar, substitute for platinum (see section 3.1.2). A Pt-$WO_3$ system has been used for the degradation of phenol.[7] This particular study did not use exclusively visible light irradiation, so it does not represent the ideal study of photocatalytic activity (which would include exclusively visible light or simulated sunlight). Pt was chosen as a dopant based on past success doping $TiO_2$ with platinum.

A platinum coated $WO_3$ catalyst was prepared by broad irradiation of a suspension of $WO_3$ in an aqueous solution of $H_2PtCl_6$ in the presence of methanol (as a sacrifical electron donor).[7] Photocatalytic activity was observed to be low with bare $WO_3$ and increased as the amount of platinum deposited on the surface increased up to 2 wt%. The sample with 3% platinum showed the same photocatalytic activity as the sample with 2% platinum. Degussa P25, a commercially available $TiO_2$ photocatalyst, often considered the "gold standard" with which to compare photocatalyst activity, was also studied under the same set of conditions in order to draw comparisons between the titanium dioxide and tungsten trioxide photocatalysts. P25 was able to achieve complete mineralization of phenol in ca. 2.5 h, much faster than either anatase $TiO_2$ (Merck) or 2 % Pt-$WO_3$. 2% Pt-$WO_3$, the most photoactive of all the platinum coated tungsten trioxide catalysts was only able to achieve 94% mineralization of phenol after approximately 11 hours.[7] Some of the intermediates formed in the degradation of phenol by Pt-$WO_3$ are distinct from those formed by degradation by P25, and the distribution of common intermediates is different. Degussa P25 produces quinone, muconic acid, and hydroquinone as products, with hydroquinone as the most abundant intermediate (Scheme 1). It should be noted that benzoquinone and hydroquinone are rapidly interconverted under these conditions. The concentration of all products is greatest at approximately 1 hour, with all intermediates eventually being fully degraded. Pt-$WO_3$ has a very distinct distribution of intermediates, and the major intermediate formed is different at different points in the reaction. Quinone is the major product at ca. 2 hours and is fully degraded after 8 hours of irradiation. Catechol concentration peaks at ca. 3.5 hours, though muconic acid is the major product from that point on. Catechol is fully degraded after 6 hours, when the concentration of

muconic acid peaks. After eight hours of irradiation, a significant amount of muconic acid is still present in the reaction mixture.[7]

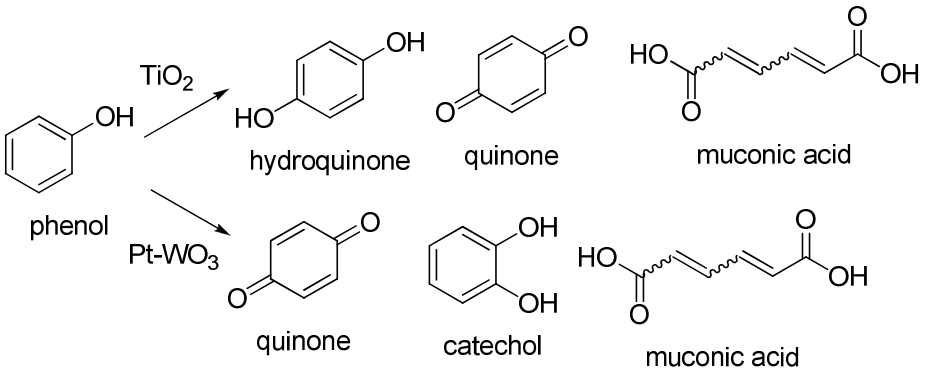


**Scheme 1. Primary degradation products of phenol.**

The more rapid degradation of phenol by $TiO_2$ than $WO_3$ or Pt-$WO_3$ may in part be explained by a greater adsorption of intermediates onto the $TiO_2$ surface, larger presence of surface hydroxyl groups, and a more significant $O_2$ adsorption.[7]

It is also thought that $WO_3$ is unsuitable as a photocatalyst because it is incapable of a one electron reduction of oxygen after irradiation with light. Although the photogenerated electrons may not be able to rapidly reduce oxygen to superoxide, they are still capable of reduction reactions. Reduction of $Fe^{3+}$, $Ag^{+}$, and $Ce^{4+}$ by $WO_3$ conduction band electrons has been previously observed.[11-13] The very fast reduction of $Pt^{4+}$ to $Pt^{2+}$ or $Pt^{0}$ during the preparation of the catalyst in this study shows that $WO_3$ photogenerated conduction band electrons are photoactive under the conditions of this study, as the same light source was used for catalyst synthesis and photocatalytic studies. The presence of platinum on the surface of the catalyst allows electrons to migrate from $WO_3$ to platinum and subsequently to $O_2$ molecules (equation 3.1), thereby increasing the photocatalytic activity.[8] The following reactions are thought to take place on the surface of the catalyst, creating a redox cycle (equations 3.1 and 3.2):

$$2O_{2(ads)} + Pt^{2+} \rightarrow 2O_{2(ads)}^{-} + Pt^{4+} \quad (3.1)$$

$$Pt^{4+} + 2_{e(cb)}^{-} \rightarrow Pt^{2+} \quad (3.2)$$

Equation 3.1 is only active for Pt-$WO_3$ catalysts with 0.5 and 1.0% Pt as catalysts while greater concentrations of Pt (2 and 3%) are shown to have $Pt^0$ instead of the highly unstable $Pt^{2+}$ species. Presence of Pt (0) species modifies the higher-Fermi level of $WO_3$, allowing transfer of photogenerated electrons to platinum, which then migrate to $O_2$.[7]

Platinum coated $WO_3$ has also been used for splitting water under visible light irradiation, but only in conjuction with a shuttle redox mediator, namely $IO_3^-/I^-$. Oxidation of water to $O_2$ was achieved with this system.[14] Complete oxidation of acetaldehyde under visible and UV irradiation was achieved by combining $WO_3$, an n-type semiconductor, with $CuBi_2O_4$, a p-type semiconductor.[15] $WO_3$ has also been combined with CuO to achieve complete mineralization of acetaldehyde. CuO enhances the photocatalytic activity of $WO_3$ by promoting oxygen reduction. Photoexcited electrons are transferred from $WO_3$ to CuO and Cu(II) is reduced to Cu(I), which is then reoxidized by $O_2$ in the air, creating a Cu(II)/Cu(I) redox cycle.[16]

Abe and Ohtani recently reported a platinum-loaded $WO_3$ catalyst with greatly improved visible light activity.[17] Platinum-loaded $WO_3$ was prepared by a photodeposition method from $H_2PtCl_6 \cdot 6H_2O$ onto fine particulate $WO_3$ (50-200 nm; ca. 10.5 $m^2\ g^{-1}$) under visible light irradiation in water and methanol, creating a uniform dispersion of Pt particles of approximately 5 nm on the surface of the $WO_3$ surface. This procedure is very similar to previous literature procedures for platinum deposition onto metal oxide surfaces.[7] Abe and Ohtani found Pt-$WO_3$ (1 wt% was optimal) to have greater photocatalytic activity than $TiO_2$ (Degussa P25) or N-$TiO_2$[18] for the degradation of an aqueous solution of acetic acid under full-arc irradiation from a xenon lamp ($300 < \lambda < 500$ nm) and from visible light irradiation ($400 < \lambda < 500$ nm). While $TiO_2$ showed negligible $CO_2$ generation under visible irradiation, Pt-$WO_3$ exhibits high photoactivity, with a rate close to that under full arc irradiation. N-$TiO_2$ did show some $CO_2$ evolution; the rate was much lower that Pt-$WO_3$.

The degradation of acetaldehyde in the gas phase was also studied with these catalysts. Under visible irradiation with 0.1 wt% Pt-$WO_3$, the concentration of acetaldehyde decreased rapidly, accompanied by an increase in $CO_2$. The final molar amount of $CO_2$ is twice that of acetaldehyde injected, indicating a complete decomposition of acetaldehyde to $CO_2$. N-$TiO_2$ also produces $CO_2$ under the same set of conditions, but at a rate approximately 14 times lower than Pt-$WO_3$. Bare $WO_3$ was also shown to appreciably degrade acetaldehyde to $CO_2$, but saturated after only 20 minutes, likely due to the accumulation of intermediates on the surface of the catalyst. 0.5 wt% Pt-$WO_3$ was also found to completely degrade isopropyl alcohol to $CO_2$ after only 30 minutes of full arc irradiation or 90 minutes of visible irradiation.

Photoacoustic (PA) studies of $WO_3$ reveal an upward shift in the visible region attributed to the formation of $W^{5+}$ by trapping of photoexcited electrons by $WO_3$[17]. Under UV irradiation in a $N_2$ atmosphere the PA signal rapidly increases and then decreases slowly again in the dark. In the presence of $O_2$, formation of $W^{5+}$ is suppressed, indicating that photogenerated electrons are consumed by electron transfer to $O_2$. Addition of a small amount of Pt (0.05%) enhances $W^{5+}$ decay in the dark, but formation of $W^{5+}$ is not observed under UV irradiation in the presence of $O_2$ for catalysts loaded more than 0.5 wt% Pt. This indicates that photogenerated electrons in $WO_3$ can react efficiently with $O_2$ before being trapped to form $W^{5+}$, and that the presence of platinum accelerates this reaction. These results strongly suggest that the photoexcited electrons in $WO_3$ are reactive towards $O_2$, and especially so when coated with platinum, contradicting the long-held view that the conduction band electrons of $WO_3$ are unable to reduce $O_2$.

### 3.1.2 WC-$WO_3$

While platinum has been shown to increase photocatalytic efficiency of both $TiO_2$ and $WO_3$ photocatalysts, its use is limited by expense. Hashimoto, et al, hypothesized that the presence of platinum may allow $WO_3$ to use a multielectron oxygen reduction reaction (ORR) pathway. Under this assumption, Hashimoto, et al attempted to synthesize a doped $WO_3$ catalyst capable of the multielectron oxygen ORR pathway using a less expensive

dopant, namely tungsten carbide. It has been previously suggested that WC can serve as an ORR catalyst.[19-21] The electronic density of states near the Fermi level of WC is similar to that of Pt.[22-24] WC is resistant to catalytic poisoning with specific oxygen adsorption[25] and has a work function of 5.0 eV.[26] All of these desirable characteristics make WC currently the most promising replacement for Pt.

A WC/$WO_3$ composite photocatalyst was prepared by mechanical mixing of $WO_3$ and 0.6 wt% WC in a mortar for 1 hour and its ability to degrade isopropanol under visible light irradiation was studied.[27] The addition of tungsten carbide did not move the absorption edge to longer wavelengths, but did increase the amount of light absorbed at wavelengths longer than the main absorption edge (approx. 460 nm; 2.6 eV) compared to $WO_3$. The concentration of acetone steadily increased to a maximum at 55 hours and then slowly decreased. $CO_2$ evolution increased slowly until the maximum concentration of acetone was reached, after which the rate of $CO_2$ production greatly accelerated. The acceleration of the isopropanol degradation by the presence of WC is highly suggestive of the ability of tungsten trioxide to serve as an ORR catalyst in place of platinum.

The research presented in this thesis seeks to expand upon the current knowledge concerning tungsten trioxide and tungsten carbide-tungsten trioxide composite photocatalysts. In the current preliminary study, the photocatalytic activity of $WO_3$ and WC-$WO_3$ was studied using quinoline as a probe molecule. Quinoline is used as a probe molecule because of the difference in electron density between the two rings which allows observation of products results from electrophilic attack of hydroxyl radicals on the benzene ring and products from single electron transfer (SET) and has well-established chemistry.[28] At present, there exists no literature on the degradation of quinoline with $WO_3$ photocatalysts, and thus the experimental results presented here will aid in understand the photochemistry of $WO_3$ photocatalysts.

## 3.2 Experimental Procedure

### 3.1.1 Organic Materials

Quinoline was used as purchased from Sigma-Aldrich without further purification. Water was purified using a Milli-Q UV plus system with a resistivity above 18 MΩ/cm.

### 3.2.2 Catalyst Preparation

$WO_3$ (<100 nm) was used as received from Sigma-Aldrich. The 0.6 wt% WC-$WO_3$ was prepared in a manner similar to a literature procedure.[27] WC (6.0 mg; Sigma-Aldrich, used as received) was ball milled with $WO_3$ (1.00 g; Sigma-Aldrich, <100 nm; used as received) using a tungsten carbide SPEX 8000 Ball Mill with four small and one large tungsten carbide balls for 15 minutes.

### 3.2.3 Catalyst Characterization

Powder x-ray diffraction (XRD) spectra were taken with a x-ray powder diffractometer employing Cu $K_\alpha$ radiation. Diffuse reflectance spectra (DRS) were generated with a UV-vis spectrometer equipped with a diffuse reflectance accessory.

### 3.2.4 Photocatalytic Measurements

Reaction mixture preparation, photolysis conditions, and analysis procedures were similar to previous work by the Jenks group.[29] The suspensions contained tungsten trioxide or tungsten carbide-tungsten trioxide composite at a concentation 1.00 mg/mL. The initial concentrations of quinoline was 0.15 mM and the solution was maintained at pH 6.0 ± 0.5 or pH 3.0 ± 0.5. The pH was adjusted and maintained over the photolysis by careful addition of aqueous NaOH or $HNO_3$. The solution was purged with $O_2$ and stirred in the dark for a minimum of 30 minutes before reactions. Reactions were irradiated with 350 nm broad range 4-Watt bulbs in a Rayonet minireactor or 420 nm bulbs in a Rayonet reactor. All photolyses were carried out at ambient temperature with continuous stirring and $O_2$ bubbling in the reaction mixture.

For kinetics, 1 mL samples were acidified with 10 μL 1*N* $H_2SO_4$, centrifuged, filtered and analyzed by HPLC. HPLC analysis was done using a C18 reverse phase column using a diode array detector. Compounds were identified by comparison to authentic samples. Quinoline and the oxidized products were easily identifiable by HPLC. However, it was determined that using two different mobile phases was ideal for analysis of products, as overlap between product peaks made analysis difficult. For HPLC analysis of quinoline, 4-quinolinone (**4HQ**), 2-aminobenzaldehyde (**2AB**), and 2-quinolinone (**4HQ**) 1:3 methanol:water with 0.2% acetic acid was used as the mobile phase. Analysis of 5-hydroxyquinoline (**5HQ**) and 8-hydroxyquinoline (**8HQ**) was done using 1:9 methanol:water with 0.2% acetic acid mobile phase with an elution rate of 0.75 mL/min.

## 3.3 Results

### 3.3.1 Catalyst Characterization

XRD revealed that the structure of $WO_3$ was monoclinic (Figure 1). The peak broadening in WC-$WO_3$ compared to $WO_3$ indicates that the WC-$WO_3$ maintains a monoclinic structure, but the particle size is smaller in the composite photocatalyst, as would be expected after ball-milling. DRS revealed that the WC-$WO_3$ composite photocatalyst had a greater absorption in the visible range, though the band gap edge was not appreciably changed (Figure 2).

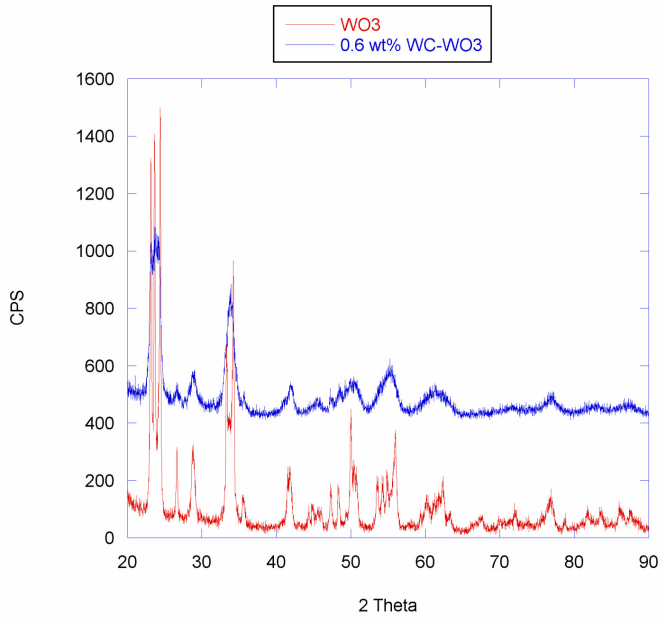


**Figure 1. XRD of $WO_3$ and WC-$WO_3$.**

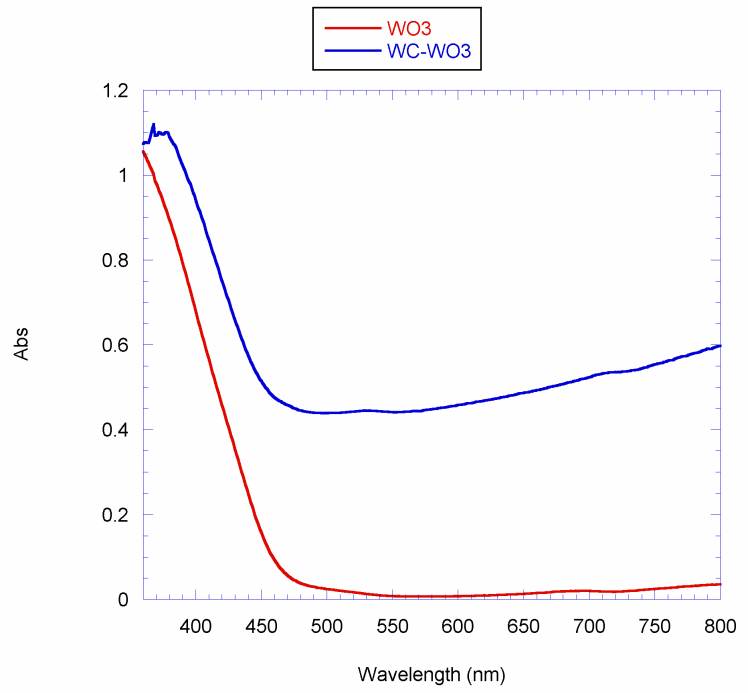


**Figure 2. DRS of $WO_3$ and WC-$WO_3$.**

### 3.3.2 Photocatalytic Experiments

Quinoline was chosen as a probe molecule for the study of these photocatalysts due to its well-established chemistry with titanium dioxide, which enables a direct comparison to the photocatalytic activity and product distribution of titanium dioxide and doped titanium dioxides, such as those studied in Chapter 2. Figure 3 shows the intial degradation of quinoline under UV (350 nm) and visible light (420 nm) irradiation. Control experiments showed that the organic compounds were stable under the conditions in the dark on the time scale of all reactions. The light sources were fluorescent tubes with broad irradiation centered at 350 nm and 420 nm. Thus, the latter is a mainly visible light source, while the former is an exclusively UV light source. Quinoline was successfully degraded under both UV and visible irradiation at both pH 3 and pH 6 by both $WO_3$ and WC-$WO_3$, though degradation was more efficient at pH 3 for both catalysts.

#### 3.3.2.1 Rates of Degradation

Quinoline was degraded efficiently under UV and visible irradiation by both $WO_3$ and WC-$WO_3$. Figures 3 and 4 show the initial and full kinetic traces for quinoline degradation at 350 nm and 420 nm, respectively.

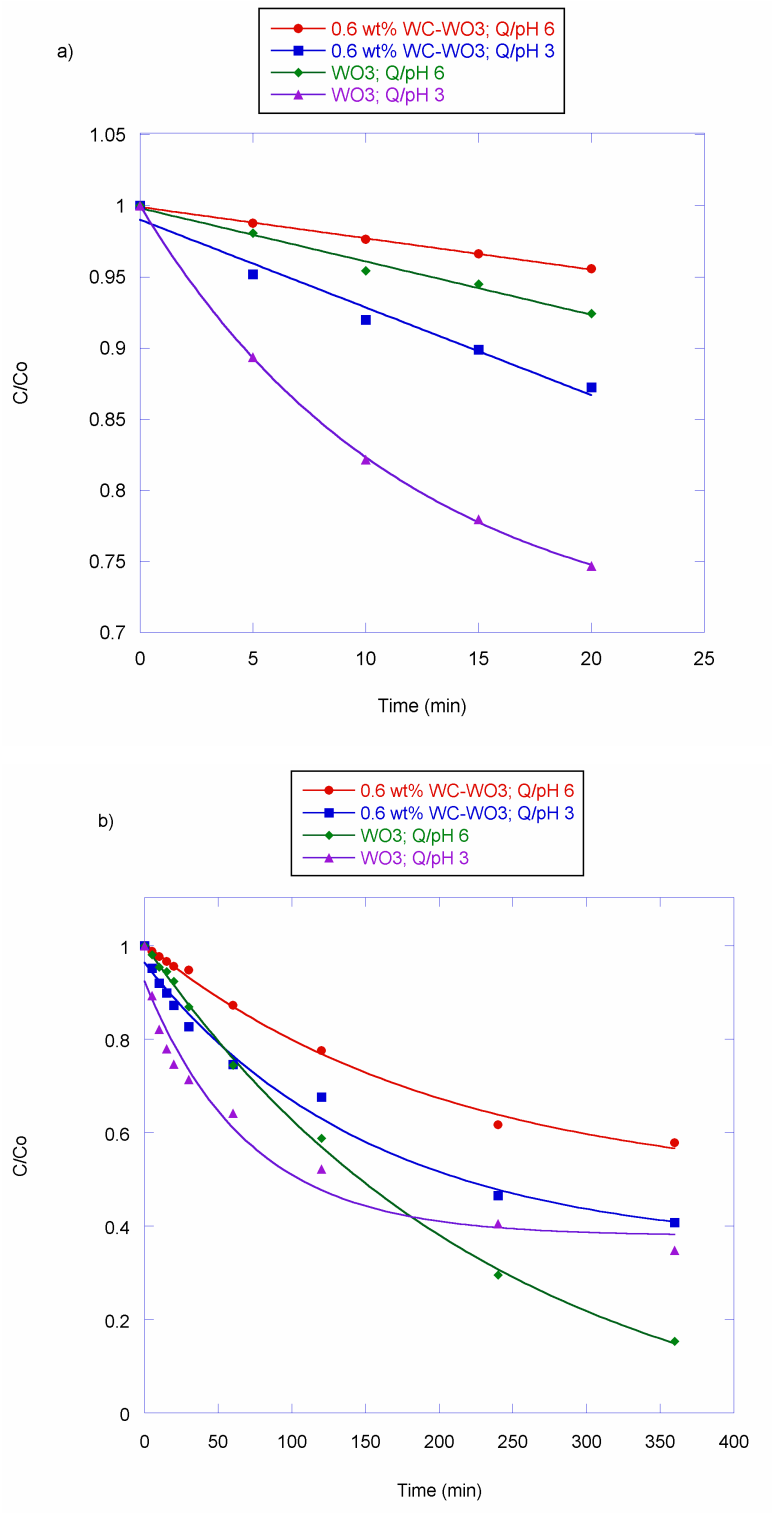


**Figure 3. Initial (a) and full kinetic (b) traces of degradation of quinoline with 350 nm irradiation.**

Both catalysts degrade quinoline faster at pH 3 than pH 6, and $WO_3$ degrades quinoline faster than WC-$WO_3$ under the same conditions with 350 nm irradiation. In the initial zero-order kinetics regime the rate of degradation is approximately 2 times faster for $WO_3$ than WC-$WO_3$ under both set of conditions. Each catalyst also degrades quinoline approximately 3 times faster at pH 3 than at pH 6.

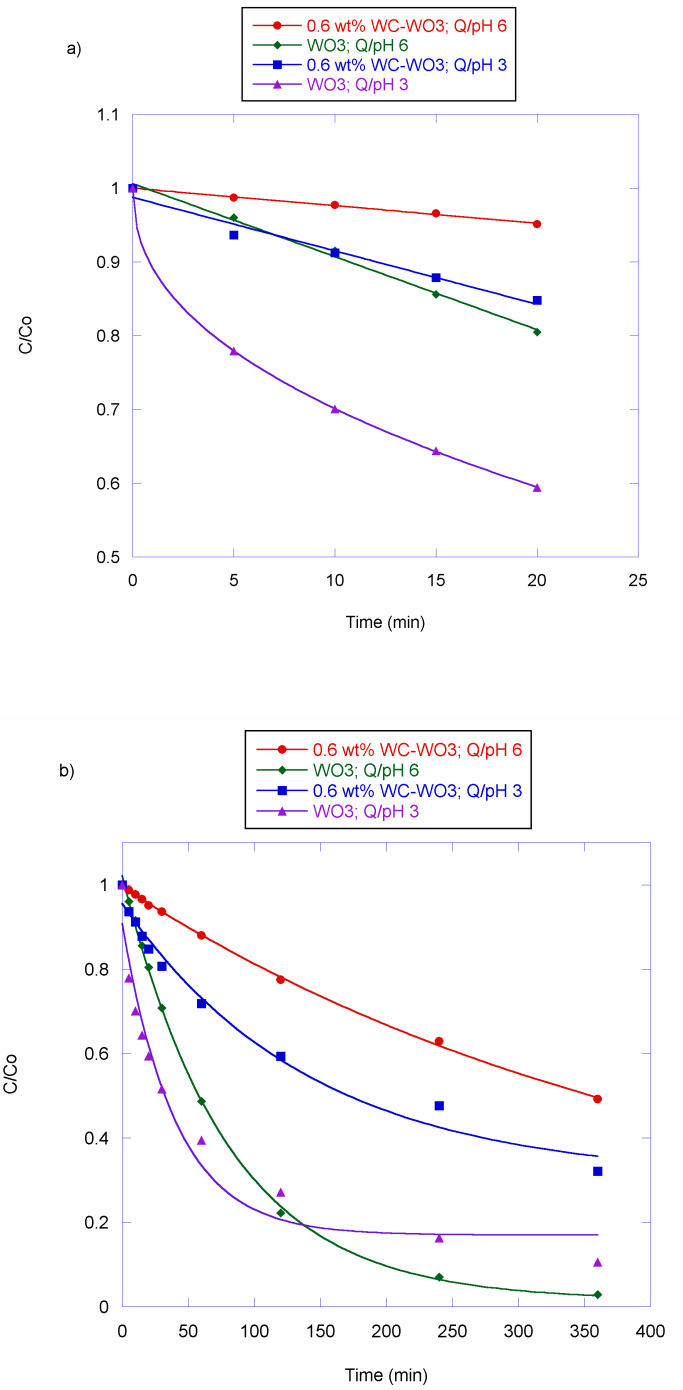


**Figure 4. Initial (a) and full kinetic (b) traces of degradation of quinoline with 420 nm irradiation.**

Under 420 nm irradiation, $WO_3$ is superior to WC-$WO_3$ under any conditions. In the initial zero-order kinetics regime the rate of degradation is approximately 3 times faster

for $WO_3$ than WC-$WO_3$ at pH 6 and 2 times faster at pH 3. $WO_3$ degrades quinoline ca. 2.5 times faster at pH 3 than pH 6 and the rate of quinoline degradation is approximately 4 times faster at pH 3 than pH 6 for WC-$WO_3$.

### 3.3.2.2 Product Analysis

Analysis of product mixtures can provide useful, if qualitative information, about the relative rates of formations of initial degradation products and the dominant chemical pathway(s) that are operative under a given set of conditions. A major concern is secondary consumption of initial products; in some cases, no intermediates can be observed as they are degraded as quickly as or much more quickly than they are formed. Quinoline, however, was in part chosen because the early degradation products are observable and can be assigned to either the single electron transfer (SET) or hydroxyl (HO) pathway. A simplified scheme for the degradation of quinoline is given in Scheme 2.

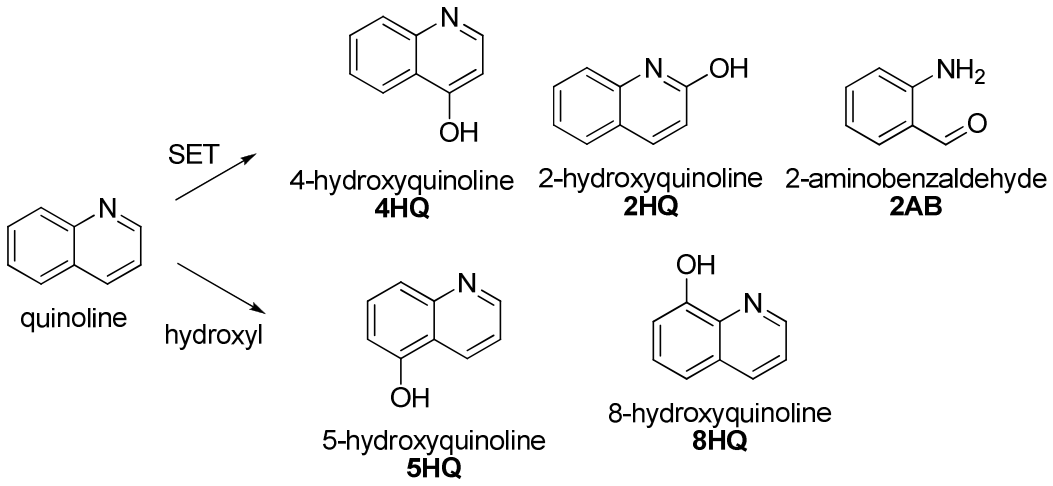


**Scheme 2. Early Photocatalytic Degradation Steps of Quinoline.**

Degradations were carried out at pH 3 and 6 for quinoline, which is below and above the pKa of quinolinium ion, respectively. Traces showing product evolution of the course of the reaction are shown in Figures 5-8. Figures 5 and 6 compares the products arising from irradiation of quinoline with $WO_3$ at pH 3 and pH 6 with 350 nm and 420 nm irradiation, respectively.

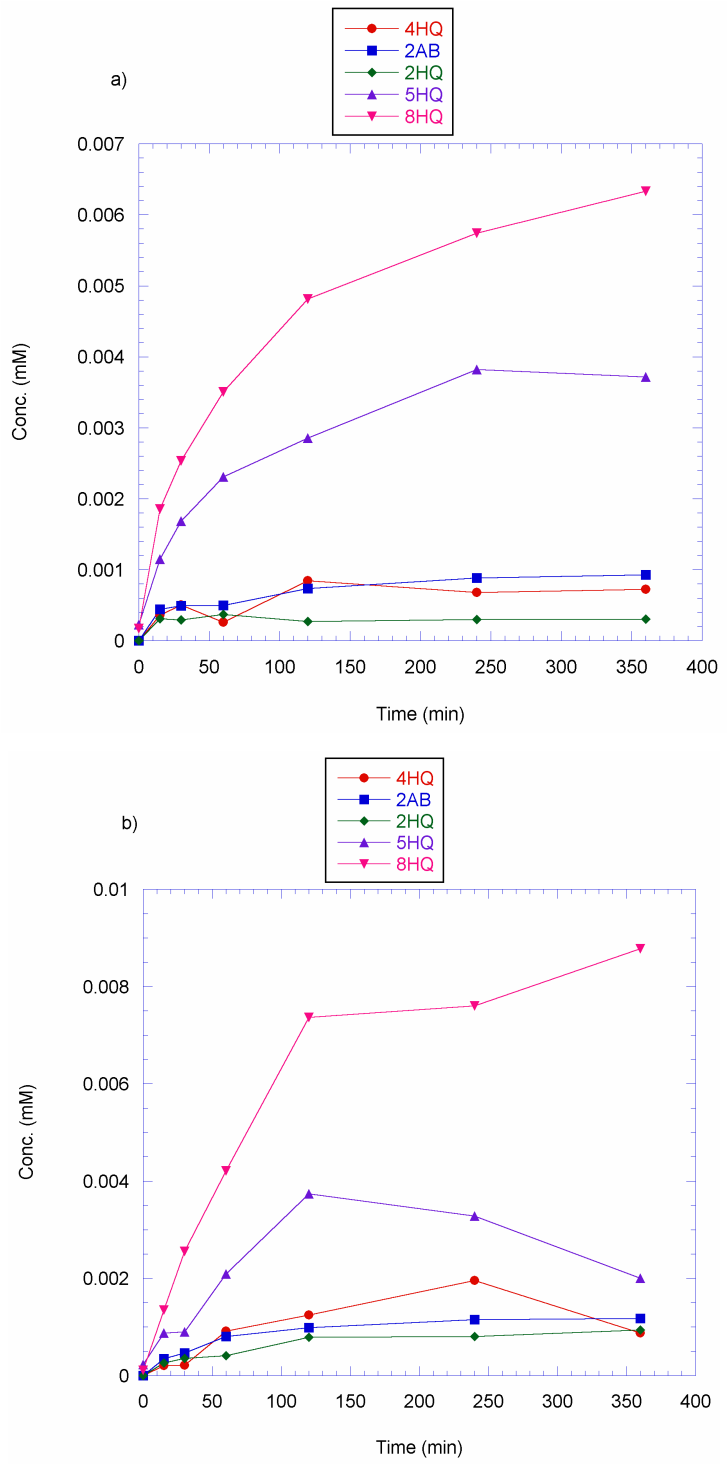


**Figure 5. Product Distribution for 350 nm photolysis of quinoline with $WO_3$ at pH 3(a) and pH 6 (b).**

Under 350 nm irradiation with $WO_3$, the hydroxyl pathway was dominant for quinoline degradation at pH 3 or pH 6, with **5HQ** as the major product. Significant amounts products from both the SET and hydroxyl pathway were formed. At pH 3, all the products were either steadily increasing or reached a plateau during the photolysis. At pH 6, two of the products, **4HQ** and **5HQ**, were degraded to some degree during the photolysis.

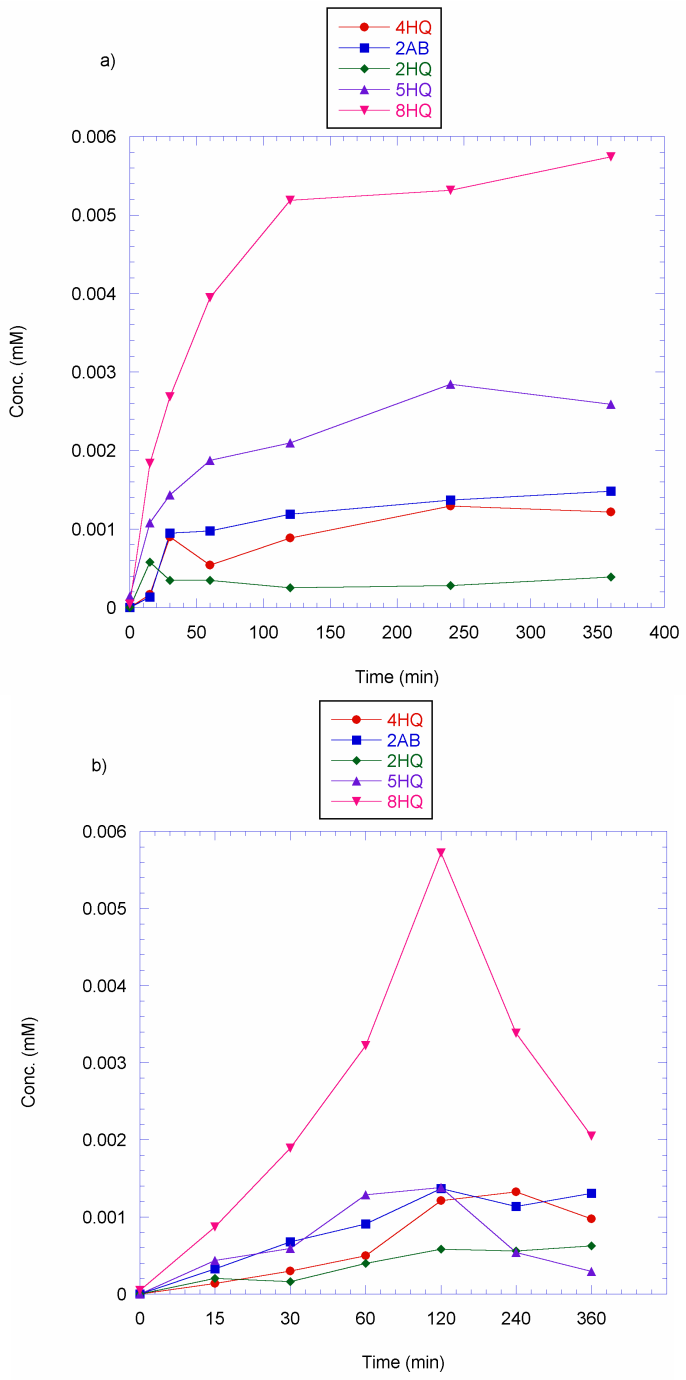


**Figure 6. Product Distribution for 420 nm photolysis of quinoline with $WO_3$ at pH 3 (a) and pH 6 (b).**

As under 350 nm irradiation with $WO_3$, the hydroxyl pathway was dominant for quinoline degradation at pH 3 or pH 6, with **5HQ** as the major product under 420 nm

irradiation. At pH 3, none of the intermediates are degraded during the course of the reaction, but **5HQ** is significantly degraded at pH 6.

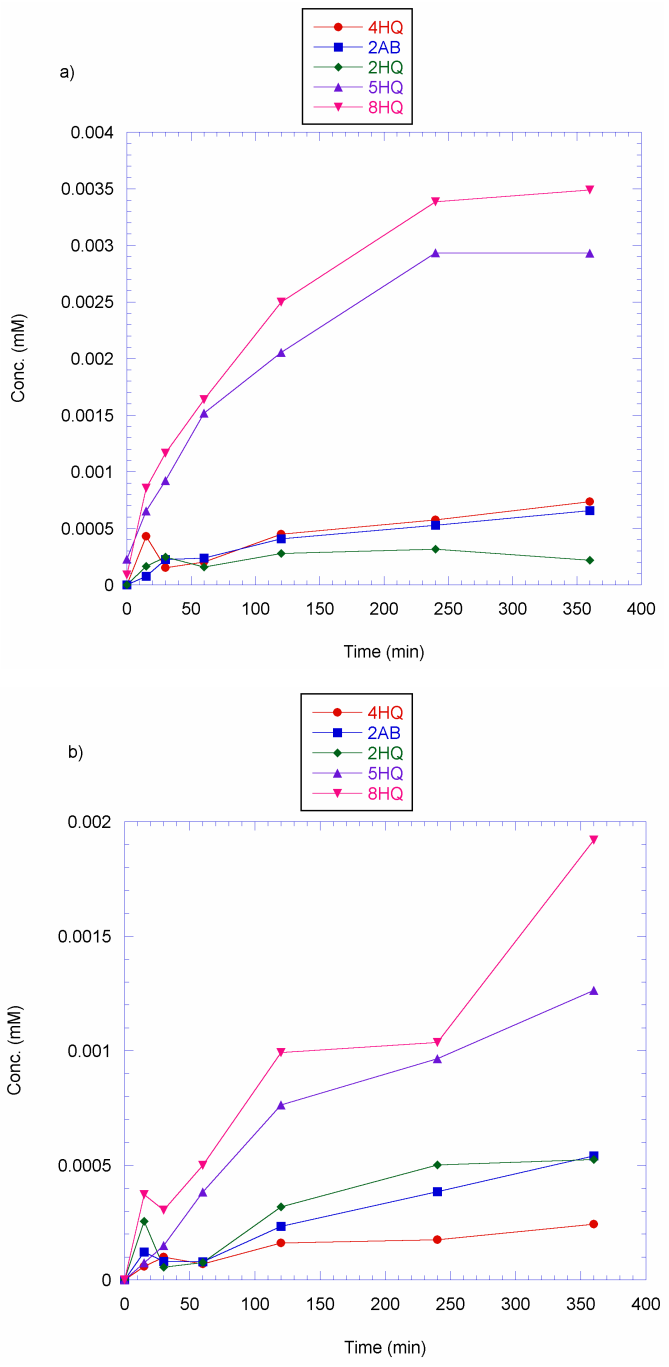


**Figure 7. Product Distribution for 350 nm photolysis of quinoline with WC-$WO_3$ at pH 3(a) and pH 6 (b).**

The hydroxyl pathway was also dominant at both pH 3 and pH 6 for WC-$WO_3$ degradation of quinoline under 350 nm irradiation. As with bare $WO_3$, intermediates built up over the course of the reaction and were not degraded.

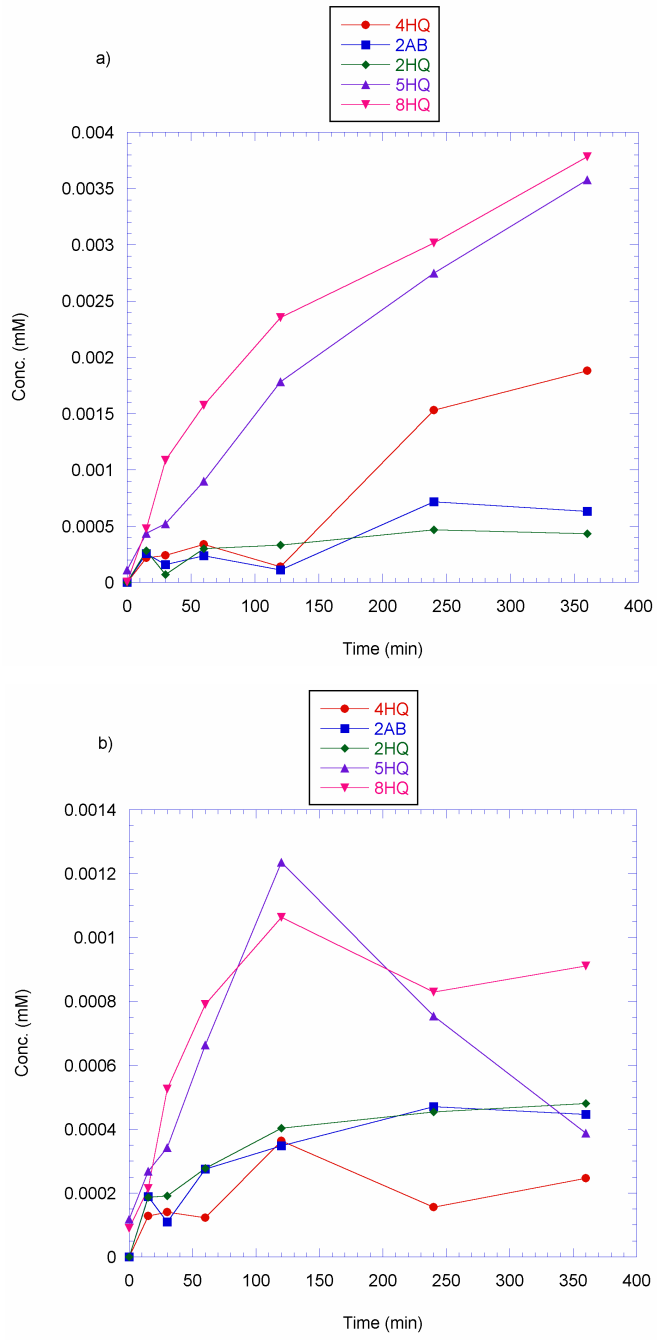


**Figure 8. Product Distribution for 420 nm photolysis of quinoline with WC-$WO_3$ at pH 3(a) and pH 6 (b).**

The hydroxyl pathway was again dominant for 420 nm photolysis of quinoline with WC-$WO_3$ at pH 3 and pH 6. At pH 6, the SET products plateaued and were not degraded further, but the HO products were both degraded to some degree over the course of the photolysis.

Hydroxyl pathway products (**5HQ** and **8HQ**) were the major products during the photolysis, regardless of the catalyst used or the reactions conditions. This is in constrast to titanium dioxide or doped titanium dioxide photocatalysts, which prefer hydroxyl products at pH 3 and SET products at pH 6 in photocatalytic degradations of quinoline. In most cases, the initial degradation products either continually increased throughout the photolysis or reached a plateau and were not further degraded during the course of the reaction. A summary of product ratios is presented in table 1.

**Table 1. Intermediate product ratios.**

| | **HO•$_{ads}$:SET intermediate product ratio**[a] | | | |
|---|---|---|---|---|
| | $WO_3$ | | WC-$WO_3$ | |
| | UV | Visible | UV | Visible |
| Quinoline, pH 6 | 3.7 | 2.2 | 2.5 | 2.1 |
| Quinoline, pH 3 | 4.1 | 3.1 | 4.0 | 2.0 |

[a]Product ratios after 2 hours of irradiation.

## 3.4 Discussion

The most important information that can be gleaned from these photocatalytic studies are general trends of reactivity, rather than specifics of each reaction. A few general trends can be drawn from these experiments that may facilitate a better understanding of the photochemistry of $WO_3$.

Quinoline leads to multiple degradation products under photocatalytic conditions, due to the difference in electronic demand in the benzene and pyridine rings. Pichat, et al,

demonstrated that electrophilic hydroxyl radicals (e.g., Fenton conditions) favor addition to the benzene ring, and SET chemistry favors functionalization of the pyridine ring and formation of **2AB** and **4HQ.**[28] Above the pKa of quinolinium, it is assumed that adsorption to the catalyst occurs mostly through the nitrogen lone pair. At low pH, quinolinium is the dominant species and not as likely to adsorb a positively charged catalyst surface (the isoelectric point of $TiO_2$ is approximately 6). Poor binding to a catalyst surface suppresses SET chemistry and increases the oxidation potential. However, since the isoelectric point of $WO_3$ is 1.5[30] quinoline is still able to adsorb to the catalyst surface, greatly increasing the rate of degradation at low pH for $WO_3$ catalysts compared to $TiO_2$ catalysts.

For both $WO_3$ and WC-$WO_3$, quinoline was degraded more efficiently at pH 3 than at pH 6 under both UV and visible irradiation, a stark contrast to titania photocatalysts. At pH 6, quinoline will not be protonated and the tungsten trioxide surface will be negatively charged (PZC (point of zero charge) is pH 1.5[30]), making adsorption to the surface less favorable and slowing the degradation. At pH 3, the tungsten trioxide surface will still be negatively charged to a great extent, and quinoline will be protonated, leading to favorable adsorption to the surface, or at the very least favorable electrostatic attraction, which would serve to bring the molecules closer in solution. In addition, titania photocatalysts tend to show a strong preference for SET products at pH 6 and hydroxyl products at pH 3. The tungsten trioxide photocatalysts presented here show a preference for hydroxyl products at all conditions studied and the preference for hydroxyl product is stronger under UV than visible irradiation (see table 1). Under most photolysis conditions, the intermediates build up, but were unable to be degraded further over the time scale of the reaction. Under some conditions primary intermediates were degraded further, so it is reasonable to assume that on a long enough time scale tungsten oxide photocatalysts would be able to degrade the primary photolysis products, at least to some extent. Titania photocatalysts, by contrast, are able to break down the intermediate compounds that are formed much more quickly. The presence of adsorbed intermediates on the $WO_3$ may also account for the reduced photoactivity compared to $TiO_2$, as the

intermediates occupy active sites that are no longer available to degrade quinoline. It is also possible that the photogenerated holes in the tungsten oxide photocatalysts do not have the oxidative power of the $TiO_2$ photogenerated holes, and thus it is more difficult for tungsten oxide photocatalysts to further oxidize the initial intermediates. Decreased adsorption of $O_2$ to the $WO_3$ photocatalyst surface compared to $TiO_2$ could account for the greater photoactivity of $TiO_2$-based photocatalysts than $WO_3$-based photocatalysts.

## 3.5 Conclusion

$WO_3$ and WC-$WO_3$ are both capable of degrading quinoline, though bare $WO_3$ shows superior activity to the WC-$WO_3$. Both catalysts show greater photocatalytic activity for the degradation of quinoline at low pH, and hydroxyl products are the major products under all conditions. Under most conditions, intermediates accumulated and were not degraded further by the photocatalyst over the course of the reaction.The bare $WO_3$ used in this study may have greater photoactivity than $WO_3$ in previous studies because the $WO_3$ used here was less than 100 nm in size, and previous studies used bulk $WO_3$[7]. The optimum size for $TiO_2$ photocatalysts is in the nanometer range,[31] so it would not be surprising to find that an optimum size also exists for $WO_3$ photocatalysts. Although the WC-$WO_3$ composite showed an increase in absorption in the visible region, it was a less successful photocatalyst. The ball milling process may have reduced the particle size (and thus increased surface area) too much, increasing the rate of electron-hole recombination and thus reducing the photocatalytic activity. Although WC-$WO_3$ did not prove to be a superior photocatalyst to $WO_3$, this study provides insight into the mechanism of photochemical degradations by $WO_3$ not known previously.

## 3.6 References

(1) Hoffmann, M.R.; Martin, S.T.; Choi, W., Bahnemann, D.W. *Chem. Rev.* **1995**, *95*, 69.

(2) Heller, A. *Acc. Chem. Res.* **1995**, *28*, 503.

(3) Fujishima, A. *$TiO_2$ Photocatalysis, Fundamentals, and Applications;* BKC: Tokyo, 1999.

(4) Abe, R.; Ohtani, B. *Kaihou Hikarishokubari* **2007**, *23*, 58.

(5) Bamwenda, G.R.; Arakawa. H. *Appl. Cat.* **2001**, *210*, 181.

(6) Hashimoto, K.; Kawai, T.; Sakata, T. *J. Phys. Chem.* **1984**, *88*, 4083.

(7) Sclafani, A.; Palmisano, L.; Marci, G; Venezia, A.M. *Sol. Energy Mater. Sol. Cells* **1998**, *51*, 203.

(8) Gerischer, H.; Heller, A. *J. Phys. Chem.* **1991**, *95*, 5261.

(9) Gerischer, H.; Heller, A. *J. Electrochem. Soc.* **1992**, *139*, 113.

(10) Wang, C.M.; Heller, A.; Gerischer, H. *J. Am. Chem. Soc.* **1992**, *114*, 5230.

(11) Erbs, W.; Desilvestro, J.; Borgarello, E.; Grätzel, M. *J. Phys. Chem.* **1984**, *88*, 4001.

(12) Desilvestro, J.; Neumann-Spallart, M. *J. Phys. Chem.* **1985**, *89*, 3684.

(13) Desilvestro, J.; Grätzel, M.; Paikossy, T. *J. Electrochem. Soc.* **1986**, *133*, 331.

(14) Abe, R.; Sayama, K.; Sugihara, H. *J. Phys. Chem. B.* **2005**, *109*, 16052-16061.

(15) Arai, T.; Yanagida, M.; Konishi, Y.; Iwasaki, Y.; Sugihara, H.; Sayama, K. *J. Phys. Chem. C.* **2007**, *111*, 7574-7577.

(16) Arai, T.; Horiguchi, M.; Yanagida, M.; Gunji, T.; Sugihara, H.; Sayama, K. *J. Phys. Chem. C.* **2009**, *113*, 6602-6609.

(17) Abe, R.; Takami, H.; Murakami, N.; Ohtani, B. *J. Am. Chem. Soc.* **2008**, *130*, 7780-7781.

(18) Irie, H.; Watanabe, Y.; Hashimoto, K. *J. Phys. Chem. B.* **2003**, *107*, 5483-5486.

(19) Mazza, F.; Trassatti, S. *J. Electrochem. Soc.* **1963**, *110*, 847.

(20) Voïnoc, M.; Bühler, D.; Tannenberger, H. *J. Electronchem. Soc.* **1971**, *118*, 1137.

(21) Lee, K.; Isihara, A.; Mitsushima, S.; Kamiya, N.; Oya, K. *Electrochim. Acta* **2004,** *49*, 3479.

(22) Levy, R.B.; Boudart, M. *Science* **1973**, *181*, 547.

(23) Colton, R.J.; Huang, J.J.; Rabalais, J.W. *Chem. Phys. Lett.* **1975**, *34*, 337.

(24) Yang, X.G.; Yang, C.W. *Appl. Phys. Lett.* **2005**, *86*, 224104.

(25) Lemaître, J.; Vidick, B.; Delmon, B. *J. Catal.* **1986**, *99*, 415.

(26) Knizkhik, A.A.; Safonov, A.A.; Iskandarova, I.M.; Bagatur'yants, A.A.; Potapkin, B.V.; Fonseca, L.R.C.; Stocker, M.W. *J. Appl. Phys.* **2006**, *99*, 84104.

(27) Kim, Y.; Irie, H.; Hashimoto, K. *Appl. Phys. Lett.* **2008**, *92*, 182107.

(28) Cermenati, L.; Pichat, P.; Guillard, C.; Albini, A. *J. Phys. Chem. B.* **1997**, *101*, 2650-2658.

(29) Li, X.; Cubbage, J.W.; Tetzlaff, T.A.; Jenks, W.S. *J. Org. Chem*. **1999,** *64*, 8509-8524

(30) Anik, M.; Cansizoglu, T. *J. Appl. Electrochem.* **2006**, *36*, 603-608.

(31) Tahiri, H.; Serpone, N.; Le van Mao, R. *J. Photochem. Photobiol. A.* **1996**, *93*, 199-203.